

CLASSIFICATION CHANGED TO

RM No 5E6J09

Source of Acquisition
CASI Acquired

Authority *H. L. Snyder* Date *12-1-60*

Dir., Aeron. Research
NACA

NACA

By *OES* (*Self Form 422*)

M. F. Schuyler

6960
Westinghouse
24C/1
12-1-60

RESEARCH MEMORANDUM

for the

Bureau of Aeronautics, Navy Department

SIMULATED ALTITUDE PERFORMANCE OF COMBUSTORS

FOR THE WESTINGHOUSE 24C JET ENGINE

I - 24C-2 COMBUSTOR

By Eugene J. Manganiello, Everett Bernardo
and Thomas T. Schroeter

Aircraft Engine Research Laboratory
Cleveland, Ohio

RESTRICTED CLASSIFICATION CANCELLED

Restriction/
Classification
Cancelled

This document contains classified information affecting the National Defense of the United States within the meaning of the Espionage Act, 18 USC 793 and 794, its transmission or revelation of its contents in any manner to an unauthorized person is prohibited by law. Information so classified may be exempted from automatic downgrading and declassification by the Secretary and Special Services of the United States. Appropriate civilian officers or employees of the Federal Government who have a legitimate interest therein, and in other States citizens of known loyalty and discretion who it is necessary must be informed thereof.

TECHNICAL
EDITING
WAIVED

OES
Status: Inactive

NATIONAL ADVISORY COMMITTEE
FOR AERONAUTICS

FILE COPY

WASHINGTON

NOV 19 1946

To be returned to
the files of the National
Advisory Committee
for Aeronautics
Washington, D. C.

RESTRICTED CLASSIFICATION CANCELLED

14

~~RESTRICTED~~ CANCELLED

NATIONAL ADVISORY COMMITTEE FOR AERONAUTICS

RESEARCH MEMORANDUM

for the

Bureau of Aeronautics, Navy Department

SIMULATED ALTITUDE PERFORMANCE OF COMBUSTORS

FOR THE WESTINGHOUSE 24C JET ENGINE

I - 24C-2 COMBUSTOR

By Eugene J. Manganiello, Everett Bernardo
and Thomas T. Schroeter

SUMMARY

A Westinghouse 24C-2 combustor was investigated at conditions simulating operation of the 24C jet engine at zero ram over ranges of altitude and engine speed. The investigation was conducted to determine the altitude operational limits, that is, the maximum altitude for various engine speeds at which an average combustor-outlet gas temperature sufficient for operation of the jet engine could be obtained. Information was also obtained regarding the character of the flames, the combustion efficiency, the combustor-outlet gas temperature and velocity distributions, the extent of afterburning, the flow characteristics of the fuel manifolds, the combustor inlet-to-outlet total-pressure drop, and the durability of the combustor basket.

The results of the investigation indicated that the altitude operational limits for zero ram decreased from 12,000 feet at an engine speed of 4000 rpm to a minimum of 9000 feet at 6000 rpm, and thence increased to 49,000 feet at 12,000 rpm. At altitudes below the operational limits, flames were essentially steady, but, at altitudes above the operational limits, flames were often cycling and either blew out or caused violent explosions and vibrations. At conditions on the altitude operational limits the type of combustion varied from steady to cycling with increasing fuel-air ratio and the reverse occurred with decreasing fuel-air ratio. In the region of operation investigated, the combustion efficiency ranged from 75 to 95 percent at altitudes below the operational limits and dropped to 55 percent or less at some altitudes above the operational limits.

~~RESTRICTED~~ CANCELLED

The deviations in the local combustor-outlet gas temperatures were within +20 to -30 percent of the mean combustor temperature rise for inlet-air temperatures at the low end of the range investigated, but became more uneven (up to ± 100 percent) with increasing inlet-air temperatures. The distribution of the combustor-outlet gas velocity followed a similar trend. Practically no afterburning downstream of the combustor outlet occurred. At conditions of high inlet-air temperature several factors indicated that fuel vapor or air formed in the fuel manifolds and adversely affected combustion. The combustor inlet-to-outlet total-pressure drop can be correlated as a function of the ratio of the combustion-air inlet density to outlet density and of the inlet dynamic pressure. The walls of the combustor basket were warped and burned during 29 hours of operation.

INTRODUCTION

An investigation of the performance of Westinghouse jet engines conducted in the Cleveland altitude wind tunnel (reference 1) revealed that the engines will not operate above a limited range of simulated altitudes for each engine speed because the combustor cannot produce gases of sufficiently high temperature for the turbine to drive the compressor. As a result of the low altitude limits of engine operation established in reference 1, a general investigation to improve the altitude performance of various models of combustor for the Westinghouse jet-propulsion engines was instituted at the NACA Cleveland laboratory at the request of the Bureau of Aeronautics, Navy Department. Reference 2 presents the simulated altitude performance of a 9.5A combustor and reference 3 presents a study of combustion performance in a 19B combustor.

The simulated altitude performance of a 24C-2 combustor, which is the first of a series of 24C combustors investigated, is reported herein. Ranges of simulated altitudes and engine speeds were investigated to determine the altitude operational limits of the 24C jet engine as indicated by the ability of a 24C-2 combustor to provide exhaust gases of the temperatures required by the turbine for engine operation. Information was also obtained regarding the character of the flames, the combustion efficiency, the combustor-outlet gas temperature and velocity distributions, the extent of afterburning, the flow characteristics of the fuel manifolds, the combustor inlet-to-outlet total-pressure drop, and the durability of the combustor basket.

COMBUSTOR

A longitudinal section of the Westinghouse 24C-2 combustor and the immediate auxiliary ducting used in this investigation is shown in figure 1. The combustor is approximately $22\frac{13}{16}$ inches long with an inside diameter of $23\frac{13}{16}$ inches and a cylindrical core $10\frac{3}{4}$ inches in diameter. The outer shell tapers to a diameter of 21 inches at the combustor outlet and the core tapers to a 13-inch-diameter section.

The combustion occurs within a basket, shown schematically in figure 2. The basket consists of two tapered concentric annular chambers having mean diameters of 14 and 21 inches, respectively. The chambers are approximately $1\frac{5}{16}$ inches wide at the upstream end and $2\frac{3}{4}$ inches wide at the downstream end and are approximately $12\frac{5}{16}$ inches long. The flame side of each shell of the annular chambers is equipped with five angular stiffener rings. The shells are perforated with 27 rows of holes lengthwise, which progressively increase downstream from $\frac{5}{32}$ - to $\frac{7}{16}$ -inch diameter, for admitting combustion air into the basket.

In each of the two annular chambers of the basket an unshielded fuel manifold is installed. A total of 60 hollow-cone-spray-type fuel-injection nozzles (45° spray angle, 7.5 gal/hr at a pressure differential of 100 lb/sq in.) is used on the manifolds, 36 on the outer and 24 on the inner manifold. Bench tests were conducted in which all 60 nozzles were calibrated with fuel in the vertically mounted manifolds. The calibrations conducted both before and after the investigation indicated a maximum individual deviation from the average fuel flow of 3 and 6 percent at fuel-manifold pressures of 25 and 5 pounds per square inch, respectively. At the low manifold pressure the flow from the bottom nozzles was higher than that from the top nozzles, which indicates that gravity affected the flow distribution.

APPARATUS

Test Setup

The general arrangement of the combustor test setup is shown in figure 3. Combustion air and fuel (AN-F-28, Amendment-2) were supplied from the laboratory systems; the fuel was filtered and fed

to the bottom of each manifold through separate inlets. Combustion-air flow and pressure were controlled with regulating valves installed in the air-supply and exhaust lines. Electric heaters were used to regulate inlet-air temperature over a low range and higher inlet-air temperatures were obtained by burning a metered amount of fuel with a portion of the air in a preheater and mixing the hot and cold streams. The preheater was operated at conditions that resulted in efficient combustion in order to minimize the contamination of the air supply. The exhaust gases from the combustor were cooled in the exit riser with water sprays and discharged into the laboratory altitude-exhaust system.

The combustion-air flow was measured with a variable-area orifice. The fuel-manifold pressure was measured at the junction of the inlets to the manifolds with a calibrated Bourdon gage and the fuel was metered with calibrated rotameters. Along one side of the combustor six sight glasses were installed for observing the combustion; another sight glass was installed downstream of the combustor to afford an axial view of the annulus (fig. 3). Immediately upstream of the combustor a plenum chamber, a punched plate (approximately 33 percent open area), and a screen (approximately 62 percent open area) were installed to correct an unsatisfactory inlet velocity distribution obtained during initial runs with a 12-inch-diameter entrance pipe; a T-section was installed at the discharge of the preheater to improve a poor inlet temperature distribution (a variation of $\pm 38^{\circ}$ F from the average) resulting from the use of the preheater. With the final inlet approach section, the variation in inlet velocity over most of the inlet was ± 2 feet per second during equilibrium flow conditions; the variation in inlet temperature was approximately $\pm 2^{\circ}$ F when the electric heaters were used and approximately $\pm 12^{\circ}$ F when the fuel-fired preheater was operated.

Temperature and Pressure Instrumentation

Temperature and pressure instrumentation was installed at five sections (A-A to E-E) shown in figure 1. The sections are designated as follows: A-A, combustor inlet; B-B, fuel-nozzle plane; and C-C, combustor outlet (corresponding to turbine-inlet section of engine); instrumentation was installed at sections D-D and E-E to check for afterburning. The orientation of the instruments within the various sections is illustrated in figure 4; all the instruments were located at approximate centers of equal areas. The numbers and types of instrument at each section are:

	Thermocouples				Total-pressure tubes			Wall static-pressure taps			
	Section				Section			Section			
	A-A	C-C	D-D	E-E	A-A	B-B	C-C	A-A	B-B	C-C	D-D
Banks	4	18	4	2	2	4	4	---	---	---	---
Probes per bank	4	4	4	2	8	3	6	---	---	---	---
Total probes	16	72	16	4	16	12	24	2	2	4	4

The construction details of the thermocouples and the pressure probes are illustrated in figure 5. The thermocouples were made of chromel-alumel wires and were connected to calibrated self-balancing indicating potentiometers through multiple switches. All of the thermocouples were unshielded except those at section E-E, which were multiple-shielded in all directions except upstream. All the air-pressure indications were obtained with banks of manometers and were photographically recorded.

METHODS AND TESTS

An investigation of the altitude operation of the 24C-2 combustor was conducted with combustion-air flow and combustor-inlet air temperature and pressure simulating operation of the jet engine at zero ram at various altitudes from sea level to 50,000 feet and for a range of engine speeds from 4000 to 12,000 rpm. Several initial runs conducted with the 12-inch-diameter entrance pipe were repeated after the entrance plenum chamber had been installed and a few of the runs in which the fuel-fired preheater caused an uneven temperature distribution were also repeated after the temperature distribution had been improved. The effect of fuel-air ratio upon combustion was observed at two conditions on the altitude operational limits. The combustion-air flow and the combustor-inlet air conditions for each operating point were obtained from estimated performance characteristics of the 24C compressor at zero ram furnished by the Westinghouse Electric Corporation, who also furnished the estimated values of the combustor-outlet gas temperatures required for operation of the 24C jet engine. Curves of these estimated values are presented in figure 6.

Ignition of a fuel-air mixture in the combustor was obtained with two spark plugs at the following approximate conditions:

Air flow, pounds per second	2
Inlet-air pressure, inches of mercury gage.	4
Fuel flow, pounds per hour.	200

After ignition was obtained, the combustion-air flow and the inlet-air temperature were set at the desired values while the fuel flow was adjusted to maintain combustion. The inlet-air pressure, initially set higher than desired, was then reduced to its proper value. In the operational runs the fuel flow was increased while all other conditions were maintained constant during an attempt to obtain an average combustor-outlet temperature equal to or greater than the value required for operation of the jet engine at the particular condition. At the two conditions at which the effect of fuel-air ratio upon combustion was observed, however, the fuel flow was independently varied over a greater range.

In most runs the combustor operating conditions were set within approximately 2 percent of the specified values; however, in several runs the attempt to set the inlet-air pressure resulted in an explosive cycling condition that induced violent vibrations in the setup and either rendered operation hazardous or caused the flames to be extinguished (blow-out). When cycling combustion did occur, several checks were made to ascertain that the combustor could not be operated at the desired point. At several such points the combustor was subsequently operated with the inlet-air pressure purposely set high to aid in establishing the altitude operational limits.

Average temperatures, total pressures, and static pressures were taken as the average of all the respective readings at each section. Average inlet and outlet velocities were calculated from air flow, areas, average static pressures, and average temperatures at sections A-A and C-C, respectively. The local combustor-outlet gas velocities used to obtain the velocity distributions were calculated from the individual probe total-pressure indications, the wall static pressure adjacent to each total-pressure rake, and the local temperatures interpolated from the indications of the adjacent thermocouple rakes. Fuel-manifold pressure differential was taken as the difference between the measured fuel-manifold pressure corrected for elevation to the center of the manifold and the average static pressure at section C-C. Although the average static pressure in the combustion zone at the plane of the fuel-injection nozzles should be used, the pressure at section C-C is considered a close approximation.

The combustion efficiency is defined as the ratio of the average gas-temperature rise through the combustor to the temperature rise theoretically obtained with the same fuel-air ratio. Values of the theoretical temperature rise were obtained from reference 4 for a fuel having a hydrogen-carbon ratio of 0.175 and a lower heating value of 18,700 Btu per pound.

The following symbols are used:

- σ_A ratio of air density at section A-A to standard NACA sea-level density
- σ_C ratio of gas density at section C-C to standard NACA sea-level density
- ΔP combustor inlet-to-outlet (sections A-A to C-C) total-pressure drop, inches mercury
- W combustion-air flow, pounds per second
- q effective dynamic pressure, inches mercury

The effective dynamic pressure q was calculated using the air flow, the average inlet-air temperature and static pressure, and the maximum cross-sectional area of the combustor (354 sq in.), which in the setup is also equal to the cross-sectional area at section A-A; hence, q is also equal to the dynamic pressure at the inlet for the configuration investigated.

RESULTS AND DISCUSSION

A summary of the data and the calculated results is presented in table I. Remarks on the general operation in each run are included. Runs 1 to 14, 16, 18, and 30, in which the inlet-air velocity or temperature distribution was uneven, were repeated after improvement of these conditions and data for these initial runs are not included in the table. The required combustor-outlet gas temperatures were obtained in four of these runs with uneven inlet distributions but not in the corresponding repeat runs. Factors that may possibly account for this adverse change in operation are the improvement of the inlet distributions and the warping of the basket; warping will be subsequently discussed. Because the inlet-air pressures were set high in runs 15, 17, and 28, the actual conditions of operation correspond to simulated-altitude and engine-speed points other than those attempted; both the attempted and the actual points are listed.

Altitude Operational Limits

The altitude operational results for zero ram are presented in figure 7 mapped on a plot of simulated altitude against simulated engine speed. The data presented are from the runs made with the final inlet-approach section; the run numbers for each point are included for convenience in referring to table I. The solid curve separates the inoperable region from the region in which the required combustor-outlet temperatures were attainable and delineates the altitude operational limits. The altitude operational limit decreases from 12,000 feet at an engine speed of 4000 rpm to a minimum of 9000 feet at an engine speed of 6000 rpm and increases with further increase in engine speed until an altitude of 49,000 feet at 12,000 rpm (military rated engine speed) is attained. In the low range of engine speeds combustion was very sensitive to changes in altitude and in this speed range the operational limit was determined within 1000 feet of altitude. The operational limit over the range of engine speeds from approximately 6600 to 9900 rpm was interpolated and is shown by a dashed line. The investigation of this range of the altitude operational limit was prevented by the laboratory-air-supply limit as indicated in the figure.

At a given simulated altitude and engine speed, the combustor inlet-air temperature and pressure increase with an increase in ram while the volume flow of air remains essentially constant. As indicated in reference 3, increases in combustor inlet-air temperature and pressure at a constant volume flow of air should improve the operation of the combustor and hence raise the altitude operational limits.

Character of Flames

Over most of the range of conditions investigated three general types of combustion were observed: steady, cycling, and flickering. Steady combustion was characterized by smooth quiet burning and blue flames, but hot spots appeared on the basket. During cycling combustion, blue and yellow flames recurrently flashed along the combustor at a frequency of approximately 8 flashes per second; the setup vibrated violently; an intermittent explosive sound occurred; and the temperatures and the pressures fluctuated. With the inception of cycling the combustor-outlet temperatures dropped 200° to 350° F; a reduction in inlet-air pressure or an increase in fuel flow during cycling combustion often resulted in blow-outs. Cycling and blow-outs occurred whether or not the spark plugs were energized. Flickering combustion usually marked the transition from steady to cycling

combustion and was accompanied by rapidly flickering flames, a moderate decrease in the combustor-outlet temperature, and the disappearance of the hot spots from the basket. In all runs the combustion was steady at altitudes below the operational limits and was either flickering or cycling at altitudes above the operational limits.

At the two conditions on the altitude-operational-limit curve (fig. 7) in which the effect of fuel-air ratio on combustion was observed, the flames flickered irregularly and intermittent partial blow-outs occurred at very low fuel-air ratios. Increasing the fuel-air ratio caused and aggravated cycling combustion and progressively intensified the vibrations and explosions in the setup to such an extent that operation was hazardous. Approximately the reverse effect on combustion was observed when the fuel-air ratio was decreased. When combustion changed from steady to cycling, a marked reduction in the rate of increase in the combustor-outlet temperatures with fuel-air ratio was noted.

Combustion Efficiency

The combustion efficiency varied from approximately 80 to 93 percent at altitudes below the operational limits (steady combustion) and from approximately 75 to 80 percent at altitudes above the operational limits during flickering combustion; during cycling combustion the efficiency dropped to 55 percent or less. For each simulated engine speed investigated, increasing the simulated altitude resulted in reduced combustion efficiency.

Combustor-Outlet Gas Temperatures and Velocities

Temperature distribution. - In most runs with steady combustion and inlet-air temperatures at the low end of the range investigated, the local maximum and minimum outlet temperatures differed from the average by approximately 20 and 30 percent, respectively, of the mean combustor temperature rise, the deviations being less than 220° F above and 290° F below the average temperature. With increasing inlet-air temperatures, however, the local maximum and minimum outlet temperatures differed from the average by amounts progressively increasing to approximately 100 percent of the mean combustor temperature rise for some cases, the deviations approaching 800° F above and below the average temperature. Cycling combustion resulted in higher percentage deviations than those for noncycling combustion.

The circumferential mean temperature at each of the four radial positions at the combustor outlet differed from the average combustor-outlet temperature by less than 5 percent of the average combustor temperature rise in most runs.

The combustor-outlet temperature distributions are shown in figure 8 for typical steady and cycling operating conditions from runs at relatively low (60° F) inlet-air temperature (runs 24 and 25, respectively); in these runs the conditions differed only slightly in air flow and approximately 2 inches of mercury in inlet-air pressure. Radial and circumferential temperature distributions are presented in polar-coordinate plots with maximum-, average-, and minimum-temperature lines included for reference; radial distributions are shown in rectangular-coordinate plots. Figure 8 illustrates the large reduction (300° F) in the average combustor-outlet temperature effected by the change from steady to cycling combustion. The temperatures nearest the outer wall are slightly low in the cycling condition but in each condition the circumferential distribution is relatively good.

Temperature distributions for steady- and cycling-combustion conditions from runs at high (280° F) inlet-air temperature (runs 42 and 40, respectively) are shown in figure 9 in plots similar to those of figure 8. In neither run shown in figure 9 did combustion occur in the top portion of the combustor and in both runs a large vertical temperature gradient existed. The region without combustion and the temperature deviations were larger in the cycling-combustion condition than in the steady-combustion condition and are reflected in the temperature patterns shown in figure 9. The large variation in the temperatures and the absence of flames in the top part of the combustor probably result from the release of fuel vapor or air in the upper portion of the fuel manifolds because of the high inlet-air temperature in these runs. This probability is subsequently discussed.

Velocity distribution. - The velocity distributions at the combustor outlet are shown in figure 10 for the two runs for which temperature distributions are presented in figure 8 (runs 24 and 25). The double annulus of the combustor basket was reflected in a double peak in the radial velocity distribution. The greatest difference in the velocities was approximately 50 feet per second (from 305 to 355 ft/sec) in the steady condition (run 24) and approximately 70 feet per second (260 to 330 ft/sec) in the cycling condition (run 25).

Indications of afterburning from average gas temperatures. - Comparisons of the average gas temperatures, which were measured to

check for afterburning, at sections D-D and E-E with the average combustor-outlet gas temperatures at section C-C are shown in figure 11. In neither plot is there evidence of appreciable afterburning, most of the temperatures at sections D-D and E-E being the same as the corresponding temperatures at section C-C. In some of the high-temperature points at section E-E (fig. 11(b)), however, a difference of as much as 200° F exists, probably because the four thermocouples at section E-E are not adequate for a true average temperature indication; all the differences greater than 50° F occurred when the outlet-gas temperature distribution was uneven.

Fuel-Manifold Characteristics

The variation of fuel flow with fuel-manifold pressure differential is presented in figure 12 and the results are compared with the bench-test calibration of the fuel manifold. Runs in which the inlet-air temperature was above 145° F are indicated separately and a line of approximately constant inlet-air temperature (260°-290° F) is shown. For a given pressure differential the fuel flow at low inlet-air temperatures corresponds approximately to that obtained in the calibration but the fuel flow decreases with increasing inlet-air temperature; this effect was more pronounced at low pressure differentials. This reduction in fuel flow at high inlet-air temperature is believed to be caused by the collection of either fuel vapor or air in the upper portion of the manifolds and their delivery from the upper nozzles with an attendant reduction in the weight of fuel delivered as a result of the large specific volume of the vapor. A reduction in inlet-air temperature or an increase in fuel-manifold pressure differential decreased the difference between the fuel flow indicated by the calibration curve and the fuel flow observed in the tests, which indicated that the amount of liquid fuel discharged from the nozzles affected by vaporization increased with any change tending to inhibit the formation of vapor. The absence of flames in the upper portion of the combustor and the large vertical temperature gradients obtained with high inlet-air temperatures (examples shown in fig. 9) support the evidence of fuel vaporization or deaeration presented in figure 12. The lack of evidence of vapor formation in runs with low inlet-air temperature and high average combustor-outlet gas temperature indicates that for the combustor investigated the formation of vapor is affected more by the inlet-air temperature than by radiation from the flames. This effect might be expected because the manifolds are in direct contact with the combustion air on the upstream side but are somewhat shielded from the flames and consequently from radiation by the basket on the downstream side. Although the nozzles are exposed to the flames, the vapor formation in the nozzles due to

radiated heat is probably small because the time required by the fuel to pass through the nozzles is much smaller than that required to traverse the manifolds.

Correlation of Total-Pressure Drop

A correlation of the combustor inlet-to-outlet total-pressure drop (sections A-A to C-C) with the inlet-to-outlet density ratio is presented in figure 13. Inasmuch as the relation between total-pressure drop and air flow is a function not only of inlet-air density but also of the density change, the data are presented in terms of $\sigma_A \Delta P / W^2$ plotted against σ_A / σ_C . A straight line is obtained that represents the data with a scatter of about ± 5 percent. The exponent 2 of W is the value determined from a preliminary logarithmic plot of $\sigma_A \Delta P$ (combustor total-pressure drop corrected to NACA standard sea-level density) against W for a selected group of runs in which the values of σ_A / σ_C were nearly constant. The more familiar pressure-drop term $\Delta P / q$ in which the pressure drop is expressed as a multiple of the inlet dynamic pressure can be substituted for $\sigma_A \Delta P / W^2$; a multiplying factor of 2105 that results from the maximum cross-sectional area of the combustor and the NACA standard sea-level density is used. A scale of $\Delta P / q$ is included in figure 13 for convenience. The combustor total-pressure drop varied, for runs in which the required combustor-outlet temperature was obtained, from approximately 10.5 to 13 times the inlet dynamic pressure. This pressure drop is the equivalent of 2 to 5 percent of the inlet-air total pressure.

The relation established in figure 13 is cross-plotted in figure 14 in which lines of $\sigma_A \Delta P$ are plotted against W for various values of σ_A / σ_C ; the data used to establish the exponent 2 of W are included. These lines are convenient in finding pressure drop from known values of air flow, inlet-air density, and inlet-to-outlet density ratio.

Condition of Basket

The combustor basket after 29 hours of operation is shown in figure 15. The walls of the basket were warped and burned locally, the center stiffener rings on both the inner and outer shells were extensively burned, and a circumferential wrinkle had developed in each shell, although adequate end clearance had been provided for axial expansion of the shells. A rust-colored deposit was observed

on the sections of the basket from the fuel manifolds to the third stiffener ring and the rest of the basket was coated with a canary-yellow residue. The yellow residue is typical of lead oxide and by qualitative analysis the rust-colored deposit was found to contain metallic lead and iron and an oxide of nickel. The basket was slightly discolored when it was received, apparently from previous use, but it was not burned or warped.

SUMMARY OF RESULTS

The results of an investigation of the performance of a Westinghouse 24C-2 combustor in which the operation of the 24C jet engine was simulated at zero ram over ranges of altitudes and engine speeds showed that:

1. The operation of a 24C jet engine with a 24C-2 combustor would be limited at zero ram to an altitude decreasing from 12,000 feet at an engine speed of 4000 rpm to a minimum of 9000 feet at an engine speed of 6000 rpm and increasing to an altitude of 49,000 feet at an engine speed of 12,000 rpm.

2. At altitudes below the operational limits, flames were essentially steady but at altitudes above the operational limits flames were often cycling and either blew out or caused violent explosions and vibrations.

3. At conditions on the altitude operational limits the type of combustion varied from steady to cycling with increasing fuel-air ratio and the reverse occurred with decreasing fuel-air ratio.

4. The combustion efficiency ranged from 75 to 95 percent at altitudes below the operational limits and dropped to 55 percent or less at some altitudes above the operational limit.

5. The deviations in the local combustor-outlet gas temperatures were within +20 to -30 percent of the mean combustor temperature rise for inlet-air temperatures at the low end of the range investigated but became more uneven (up to ± 100 percent) with increasing inlet-air temperatures. The distribution of the combustor-outlet gas velocity followed a similar trend.

6. Practically no afterburning downstream of the combustor outlet occurred.

7. At conditions of high inlet-air temperature several factors indicated that fuel vapor or air formed in the fuel manifolds and adversely affected combustion.

8. The combustor inlet-to-outlet total-pressure drop can be correlated as a function of the ratio of the combustion-air inlet density to outlet density and of the inlet dynamic pressure.

9. The walls of the combustor basket were warped and burned during 29 hours of operation.

Aircraft Engine Research Laboratory,
National Advisory Committee for Aeronautics,
Cleveland, Ohio.

Eugene J. Manganiello
Eugene J. Manganiello,
Mechanical Engineer.

Everett Bernardo
Everett Bernardo,
Mechanical Engineer.

Thomas T. Schroeter
Thomas T. Schroeter,
Mechanical Engineer.

Approved:

Benjamin Pinkel
Benjamin Pinkel,
Physicist.

va.

REFERENCES

1. Fleming, William A.: Altitude-Wind-Tunnel Investigation of the Westinghouse 19B-2, 19B-8, 19XB-1 Jet-Propulsion Engines. I - Operational Characteristics. NACA MR No. E6E06, Bur. Aero., 1946.

2. Manganiello, Eugene J., and Bogart, Donald: Simulated Altitude Performance of Combustors for the Westinghouse 9.5 Jet Engine. I - 9.5A Combustor. NACA MR No. E6F28, Bur. Aero., 1946.
3. Childs, J. Howard, McCafferty, Richard J., and Surine, Oakley W.: A Study of Combustion Performance in a Westinghouse 19-B Combustor. NACA MR No. E6H05, Bur. Aero., 1946.
4. Turner, L. Richard, and Lord, Albert M.: Thermodynamic Charts for the Computation of Combustion and Mixture Temperatures at Constant Pressure. NACA TN No. 1086, 1946.

INDEX OF FIGURES

	Page
Figure 1. - Longitudinal section of Westinghouse 24C-2 combustor showing auxiliary ducting and instrumentation planes	F-1
Figure 2. - Schematic diagram of basket for Westinghouse 24C-2 combustor.	
(a) Section of hole arrangement, 27 holes lengthwise.	F-2
(b) Longitudinal half section	F-2
Figure 3. - Diagrammatic sketch of general arrangement of setup for Westinghouse 24C combustors.	F-3
Figure 4. - Location of instrumentation looking upstream on Westinghouse 24C-2 combustor	F-4
Figure 5. - Construction details of instrumentation on Westinghouse 24C-2 combustor.	
(a) Total-pressure rakes and static-pressure taps	F-5
(b) Thermocouple banks and shielded thermocouples	F-6
Figure 6. - Variation of combustor operating conditions with engine speed for various altitudes at zero ram from performance estimates of the 24 C jet engine by the Westinghouse Electric Corporation.	
(a) Combustor-inlet total temperature	F-7
(b) Combustor-inlet total pressure.	F-7
(c) Combustion-air flow	F-8
(d) Required combustor-outlet total gas temperature	F-8
Figure 7. - Altitude operational limits of Westinghouse 24C jet engine for zero ram as determined with 24C-2 combustor	F-9
Figure 8. - Temperature distribution at combustor outlet (section C-C, looking upstream) for typical steady and cycling operating conditions from two runs at low inlet-air temperature. Inlet-air temperature, 60° F; Westinghouse 24C-2 combustor.	
(a) Radial and circumferential distribution during steady combustion; run 24	F-10
(b) Radial distribution during steady combustion; run 24.	F-10
(c) Radial and circumferential distribution during cycling combustion; run 25.	F-11
(d) Radial distribution during cycling combustion; run 25	F-11

Figure 9. - Temperature distribution at combustor outlet (section C-C, looking upstream) for typical steady and cycling operating conditions from two runs at high inlet-air temperature. Inlet-air temperature, 280° F; Westinghouse 24C-2 combustor.

- (a) Radial and circumferential distribution during steady combustion; run 42 F-12
- (b) Radial distribution during steady combustion; run 42. F-12
- (c) Radial and circumferential distribution during cycling combustion; run 40. F-13
- (d) Radial distribution during cycling combustion; run 40 F-13

Figure 10. - Velocity distribution at combustor outlet (section C-C) for steady and cycling combustion. Westinghouse 24C-2 combustor. F-14

Figure 11. - Relation of average gas temperature at sections D-D and E-E to average combustor-outlet gas temperature at section C-C. Westinghouse 24C-2 combustor.

- (a) Section D-D F-15
- (b) Section E-E F-16

Figure 12. - Variation of fuel flow with fuel-manifold pressure differential. Westinghouse 24C-2 combustor F-17

Figure 13. - Correlation of combustor inlet-to-outlet (section A-A to C-C) to total-pressure drop. Westinghouse 24C-2 combustor F-18

Figure 14. - Combustion-air total-pressure drop from combustor inlet to outlet (section A-A to C-C). Westinghouse 24C-2 combustor. F-19

Figure 15. - Combustor basket after 29 hours of operation. Westinghouse 24C-2 combustor.

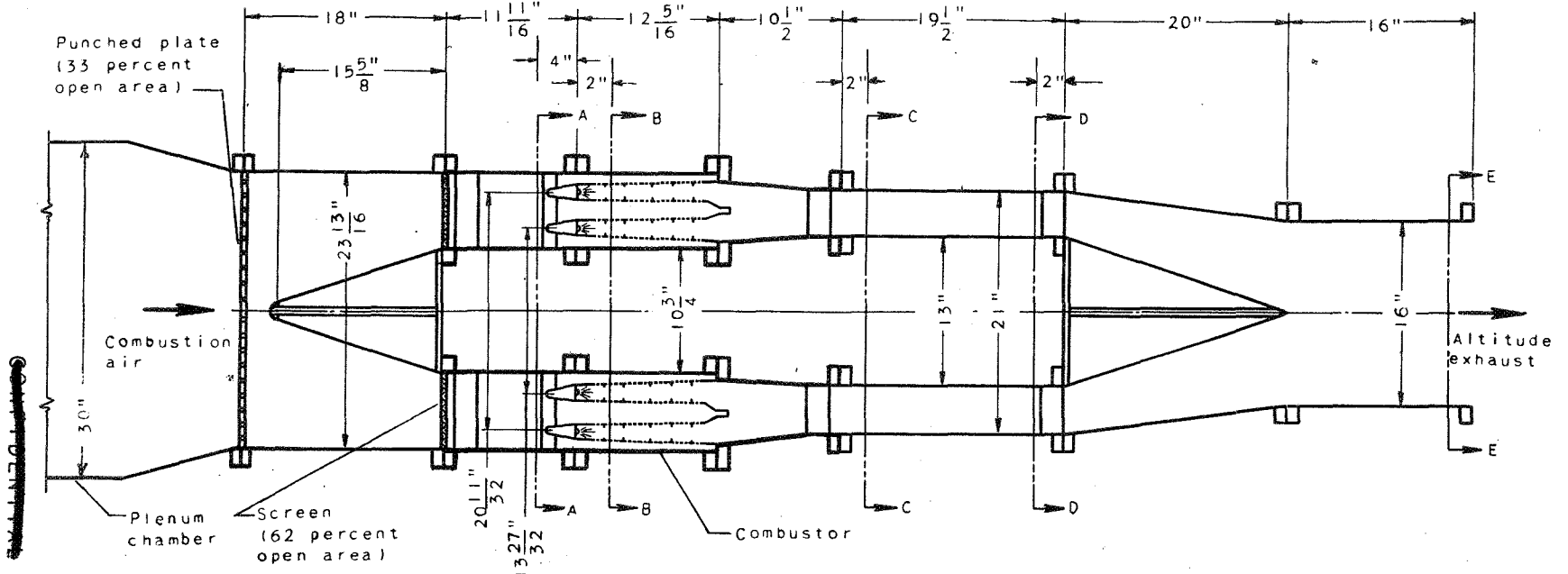
- (a) Entire basket F-20
- (b) Center shell. F-20

TABLE I - SUMMARY OF PERFORMANCE DATA OF WESTINGHOUSE 24C-2 COMBUSTOR

Run	Simulated altitude (ft)	Simulated engine speed (rpm)	Estimated required outlet total temperature (°F)	Combustion-air flow, W (lb/sec)	Inlet total temperature (°F)	Inlet total pressure (in. Hg absolute)	Fuel flow (lb/hr)	Fuel-air ratio	Fuel-manifold pressure differential (lb/sq in.)	Average outlet temperature (°F)	Maximum outlet temperature (°F)	Minimum outlet temperature (°F)
15	20,000	8,000	814	17.4	120	31.3	785	0.0126	10.0	838	980	505
17	12,800	6,850	863	15.7	104	30.2	800	.0142	10.3	957	1110	715
19	10,000	6,000	918	13.5	96	34.9	780	.0161	9.8	1107	1305	900
20	5,850	9,100	930	12.5	86	26.9	600	.0133	6.5	797	995	525
21	0	4,000	1129	11.2	149	23.7	615	.0153	7.8	961	1180	500
22	30,000	8,000	727	7.0	159	19.1	516	.0204	6.8	1211	1700	570
23	40,000	10,000	925	9.7	63	24.0	600	.0172	5.3	1045	1240	855
24	20,000	6,000	803	11.5	60	26.0	600	.0145	5.2	857	1005	570
25	20,000	6,000	803	11.9	59	24.0	597	.0138	4.9	544	700	420
26	15,000	4,000	955	8.3	45	22.1	503	.0167	4.1	953	1140	745
27	10,000	4,000	1016	9.6	63	24.1	605	.0175	5.3	1042	1260	875
28	12,000	4,000	992	9.0	55	22.7	584	.0179	5.1	1039	1220	865
29	11,400	3,960	1001	11.1	72	25.5	680	.0170	7.0	1085	1275	800
31	10,000	5,000	959	12.4	81	26.7	730	.0163	7.8	1017	1175	780
32	10,000	5,400	936	---	---	---	---	---	---	---	---	---
33	9,000	6,060	923	16.5	110	31.6	870	.0147	11.8	985	1170	840
34	10,000	6,600	907	---	---	---	---	---	---	---	---	---
35	30,000	9,400	861	17.2	141	32.5	850	.0138	11.6	931	1070	660
36	30,000	9,400	861	---	---	---	---	---	---	---	---	---
37	30,000	10,000	956	---	---	---	---	---	---	---	---	---
38	30,000	10,400	1021	17.3	188	33.1	951	.0153	15.0	1126	1335	825
39	40,000	11,000	1118	---	---	---	---	---	---	---	---	---
40	50,000	12,000	1431	8.2	282	18.0	420	.0142	10.1	829	1625	280
41	45,000	12,000	1431	10.6	272	23.5	530	.0138	13.3	1069	1860	290
42	40,000	12,000	1431	13.2	279	30.1	1060	.0224	22.6	1620	2000	885
43	40,000	11,400	1220	12.8	236	26.9	860	.0187	14.1	1365	1720	885
44	30,000	10,200	955	---	---	---	400-900	---	---	---	---	---
45	9,000	6,000	929	---	---	---	200-650	---	---	---	---	---

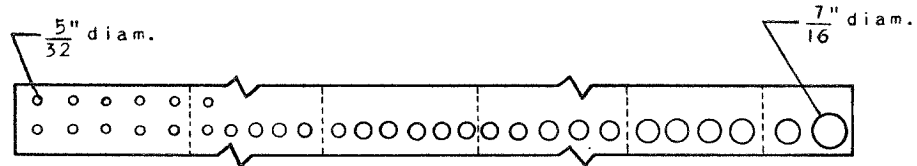
Run	Average combustor temperature rise (°F)	Combustion efficiency (percent)	Average temperature, section D-D (°F)	Average temperature, section E-E (°F)	Inlet static pressure (in. Hg absolute)	Average inlet velocity (ft/sec)	Outlet total pressure (in. Hg absolute)	Outlet static pressure (in. Hg absolute)	Average outlet velocity (ft/sec)	Inlet-to-outlet density ratio, σ_A/σ_C	Combustor total pressure drop, $\Delta P_{\Delta P}$ (in. Hg)	Condition (1)
15	718	79.1	868	850	31.2	99	29.8	28.5	401	2.44	1.48	A
17	853	83.8	969	---	30.1	90	28.9	27.8	404	2.71	1.23	B
19	1011	87.3	1105	1108	34.9	66	34.0	33.3	321	2.95	1.00	C
20	711	74.1	818	775	26.8	78	25.9	25.3	315	2.44	.79	D
21	812	75.2	965	906	23.7	88	22.9	22.1	363	2.49	.60	A
22	1052	75.1	1258	1243	19.1	69	18.6	18.2	324	2.82	.26	A
23	972	80.7	1037	1019	24.0	65	23.4	22.9	321	3.00	.57	C
24	797	77.0	867	856	25.9	71	25.2	24.6	312	2.67	.67	A
25	485	48.6	559	475	23.9	79	23.3	22.8	267	2.03	.57	B
26	908	77.0	957	953	22.1	58	21.6	21.2	282	2.92	.38	A
27	979	79.1	1033	1040	24.0	64	23.4	22.9	319	3.02	.51	C
28	984	78.2	1032	1039	22.6	63	22.1	21.6	318	3.05	.45	C
29	1013	84.5	1081	1064	25.4	71	24.7	24.0	368	3.08	.66	C
31	936	80.9	1004	973	26.6	78	25.7	25.0	374	2.92	.82	A
32	---	---	---	---	---	---	---	---	---	---	---	E
33	875	83.4	964	975	31.5	91	30.2	29.1	415	2.75	1.38	C
34	---	---	---	---	---	---	---	---	---	---	---	E
35	790	80.5	903	905	15.8	98	30.9	14.6	409	2.52	2.66	A
36	---	---	---	---	---	---	---	---	---	---	---	E
37	---	---	---	---	---	---	---	---	---	---	---	E
38	938	86.9	1132	1016	32.9	104	31.3	30.0	461	2.68	1.58	C
39	---	---	---	---	---	---	---	---	---	---	---	E
40	547	55.0	763	874	17.9	104	17.3	16.9	316	1.84	.26	B
41	797	82.0	1138	1000	23.5	101	22.7	22.1	372	2.22	.50	D
42	1341	89.6	1632	1460	30.0	99	28.7	27.5	504	3.06	1.02	C
43	1129	88.3	1376	1207	26.8	102	25.6	24.5	483	2.86	.90	C
44	---	---	---	---	---	---	---	---	---	---	---	F
45	---	---	---	---	---	---	---	---	---	---	---	F

1 Conditions indicated by letters A to F have the following significance:
 A Inlet pressure above desired value; either steady or flickering combustion; attempt to set pressure caused explosive cycling combustion.
 B Required combustor-outlet temperature not attained; either flickering or cycling combustion.
 C Required combustor-outlet temperature attained; steady combustion.
 D Required combustor-outlet temperature attainable; fuel flow arbitrarily set low; steady combustion.
 E Required combustor-outlet temperature not attained; data not recorded because of explosive cycling combustion.
 F Effect of fuel-air ratio upon combustion observed; range of variation limited by partial blow-outs; flames varied from steady through flickering to explosive cycling.

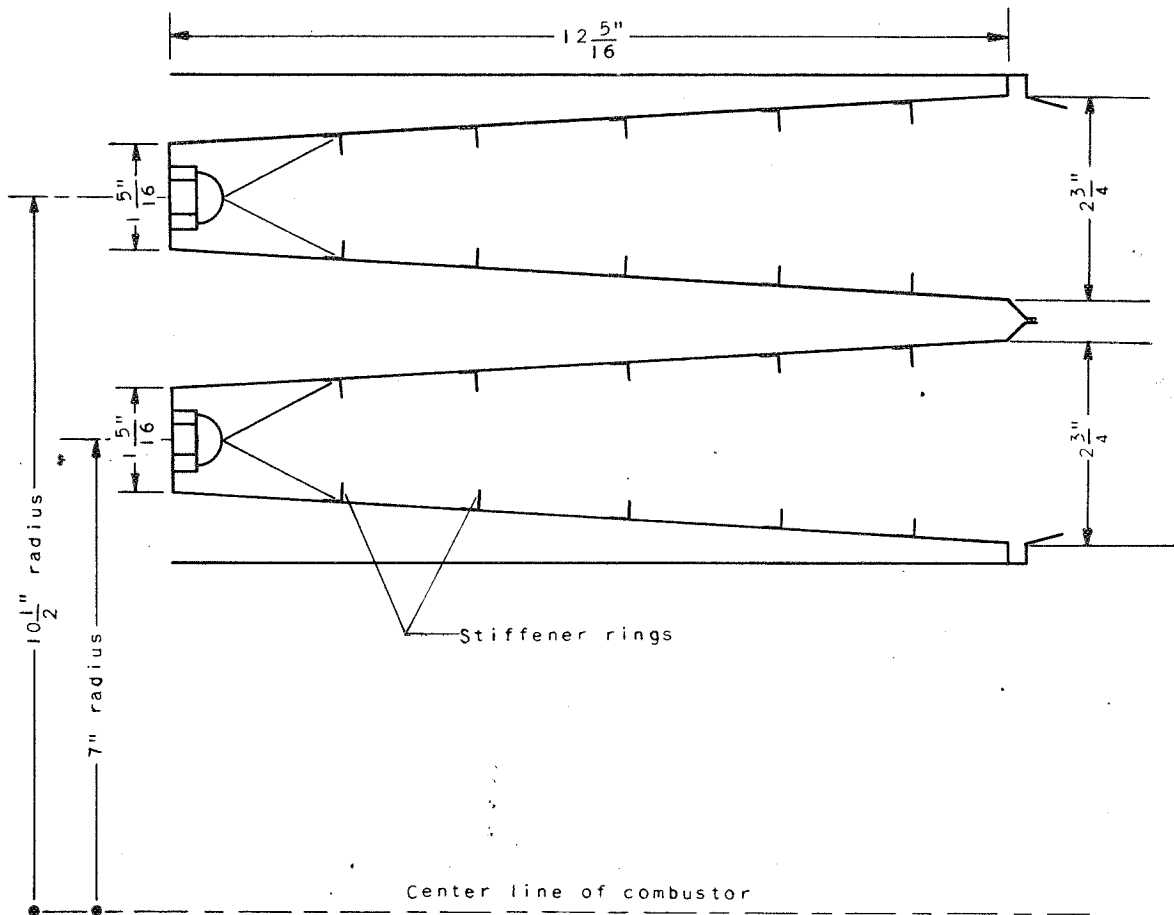


NATIONAL ADVISORY
COMMITTEE FOR AERONAUTICS

Figure 1. - Longitudinal section of Westinghouse 24C-2 combustor showing auxiliary ducting and instrumentation planes.



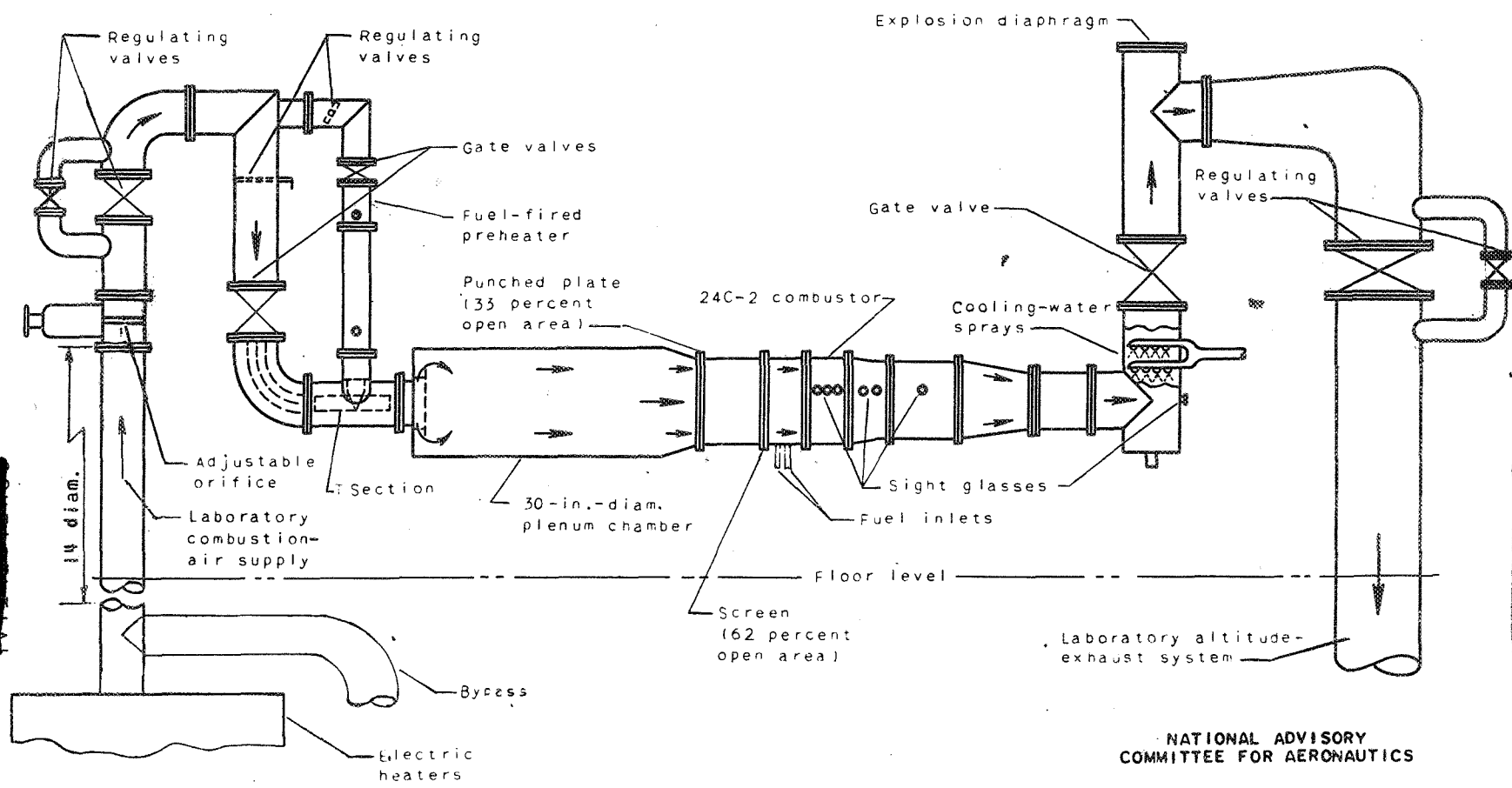
(a) Section of hole arrangement, 27 holes lengthwise



(b) Longitudinal half section.

NATIONAL ADVISORY
COMMITTEE FOR AERONAUTICS

Figure 2. - Schematic diagram of basket for Westinghouse 24C-2 combustor.



NATIONAL ADVISORY COMMITTEE FOR AERONAUTICS

Figure 3. - Diagrammatic sketch of general arrangement of setup for Westinghouse 24C combustors.

CONFIDENTIAL

CONFIDENTIAL

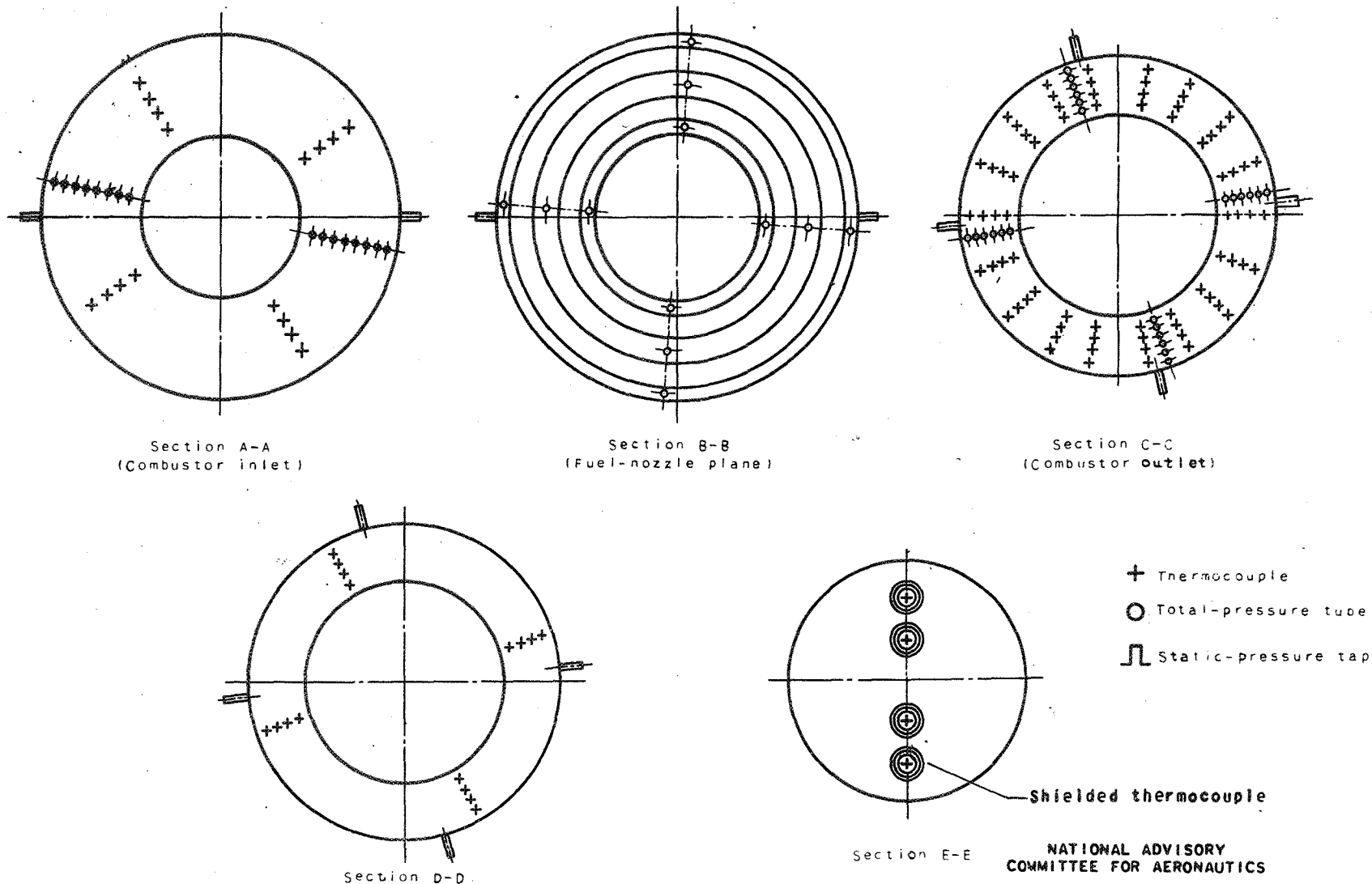
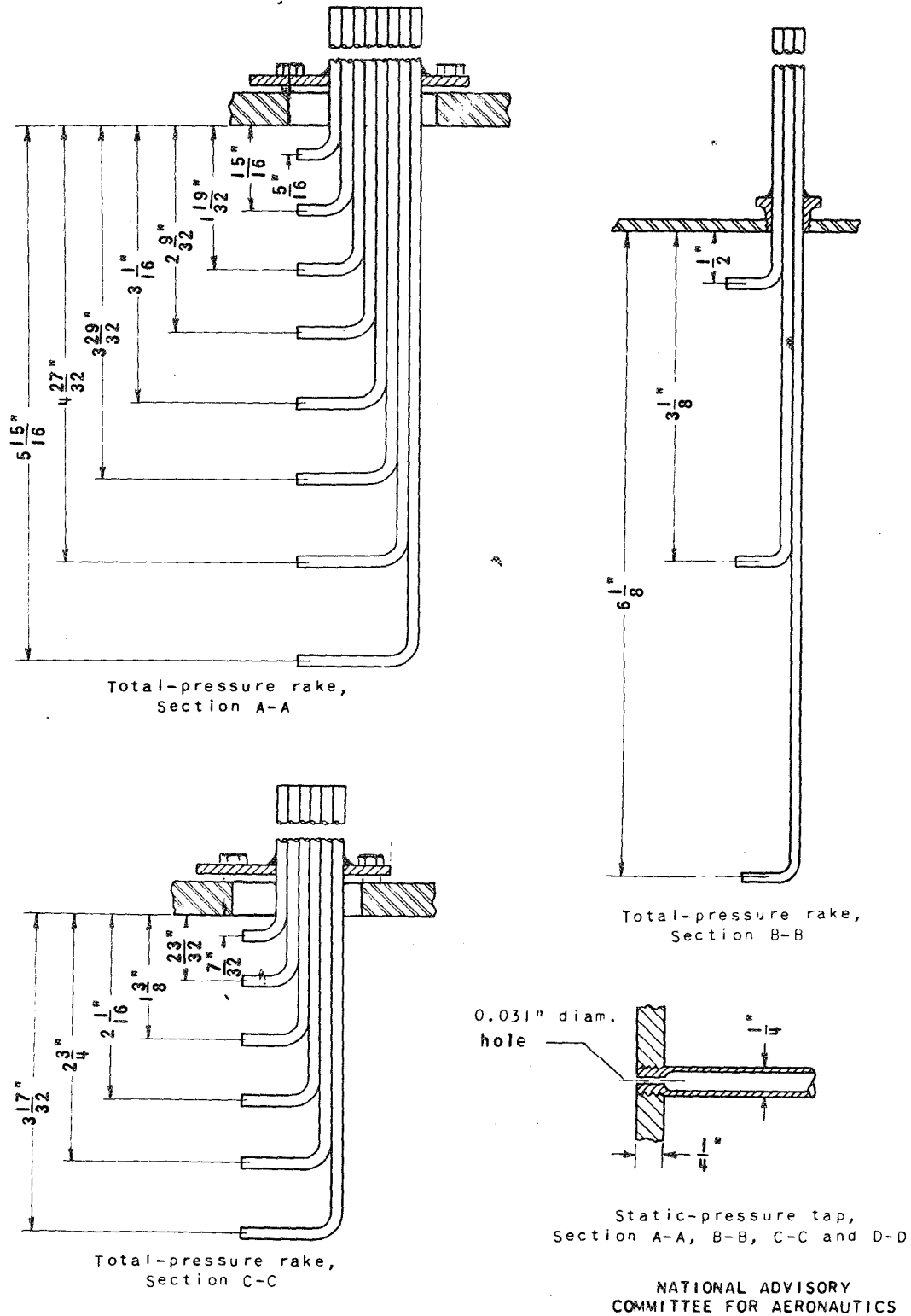
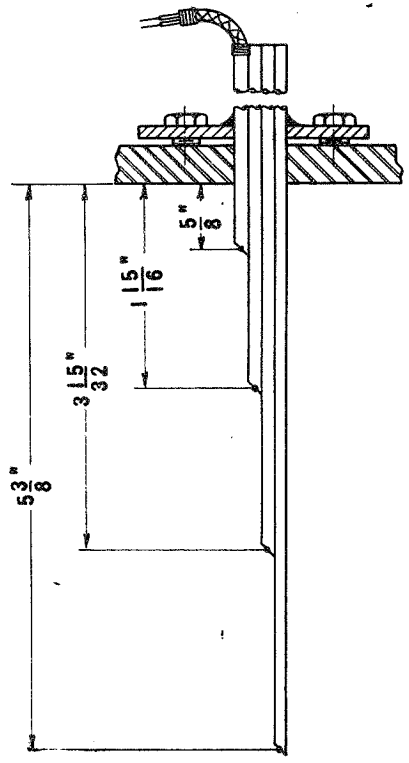


Figure 4. - Location of instrumentation looking upstream on Westinghouse 24C-2 combustor.

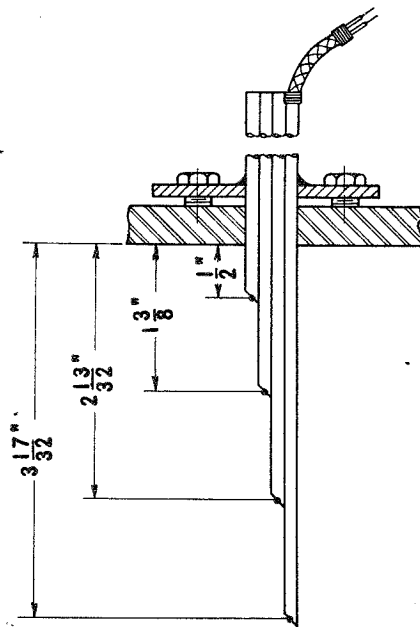


(a) Total-pressure rakes and static-pressure taps.

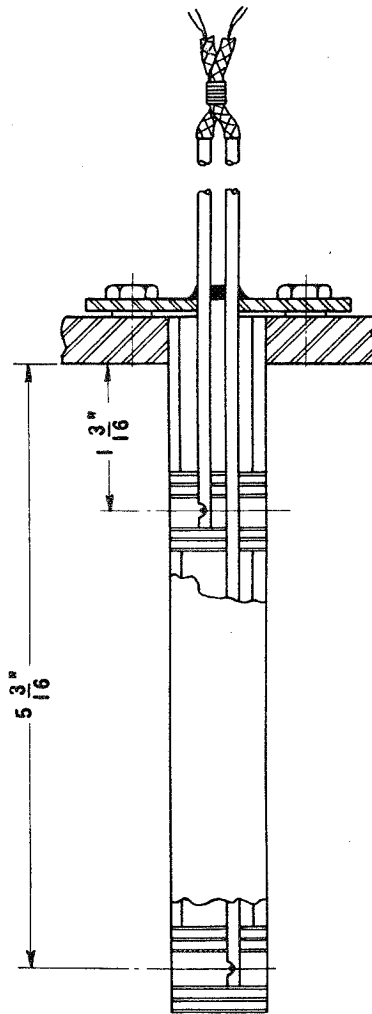
Figure 5. - Construction details of instrumentation on Westinghouse 24C-2 combustor.



Thermocouple bank,
Section A-A



Thermocouple bank,
Sections C-C and D-D

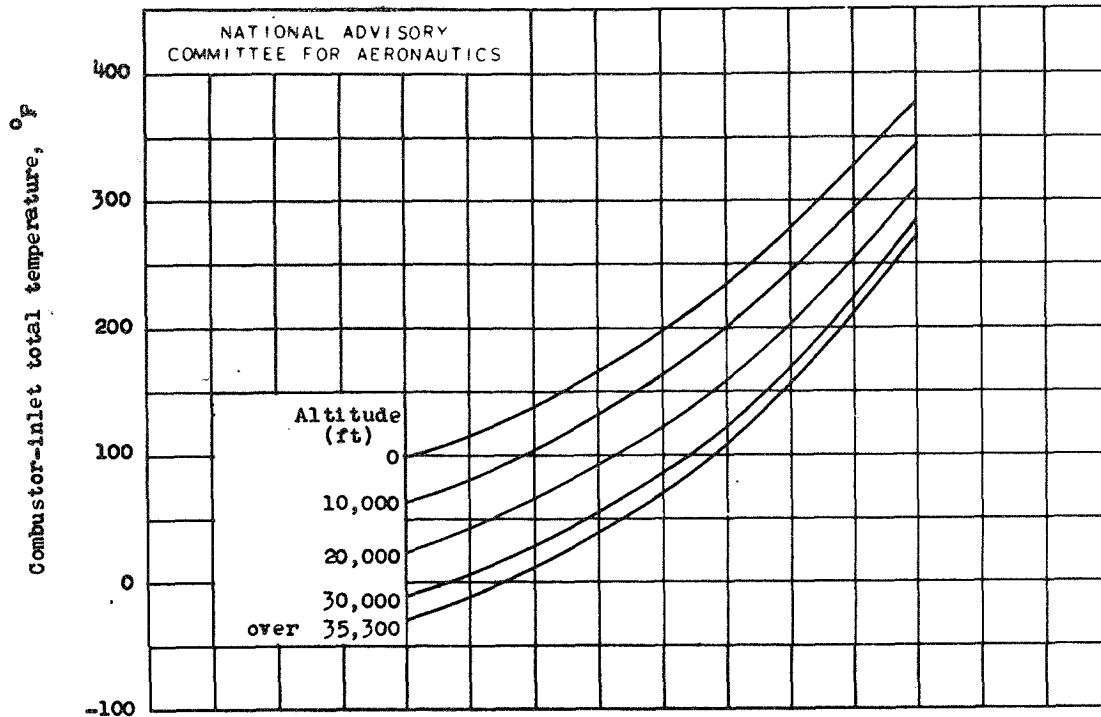


Shielded thermocouples,
Section E-E

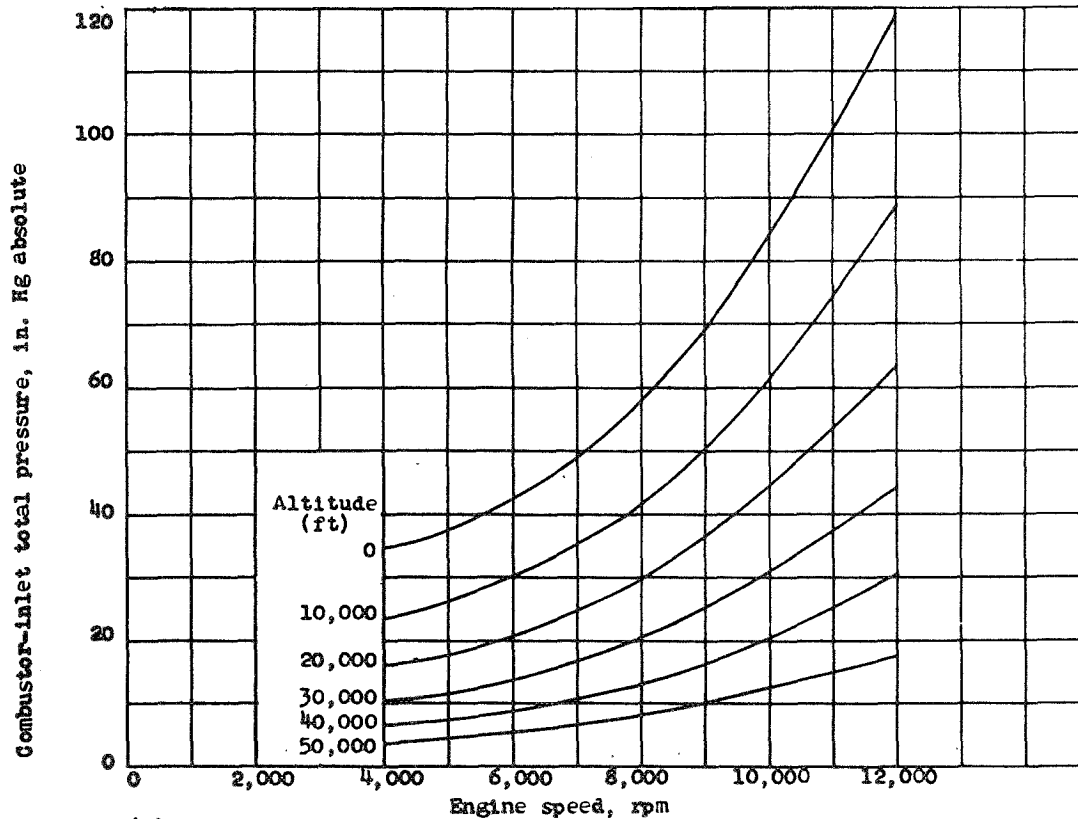
NATIONAL ADVISORY
COMMITTEE FOR AERONAUTICS

(b) Thermocouple banks and shielded thermocouples.

Figure 5. - Concluded. Construction details of instrumentation on Westinghouse 24C-2 combustor.

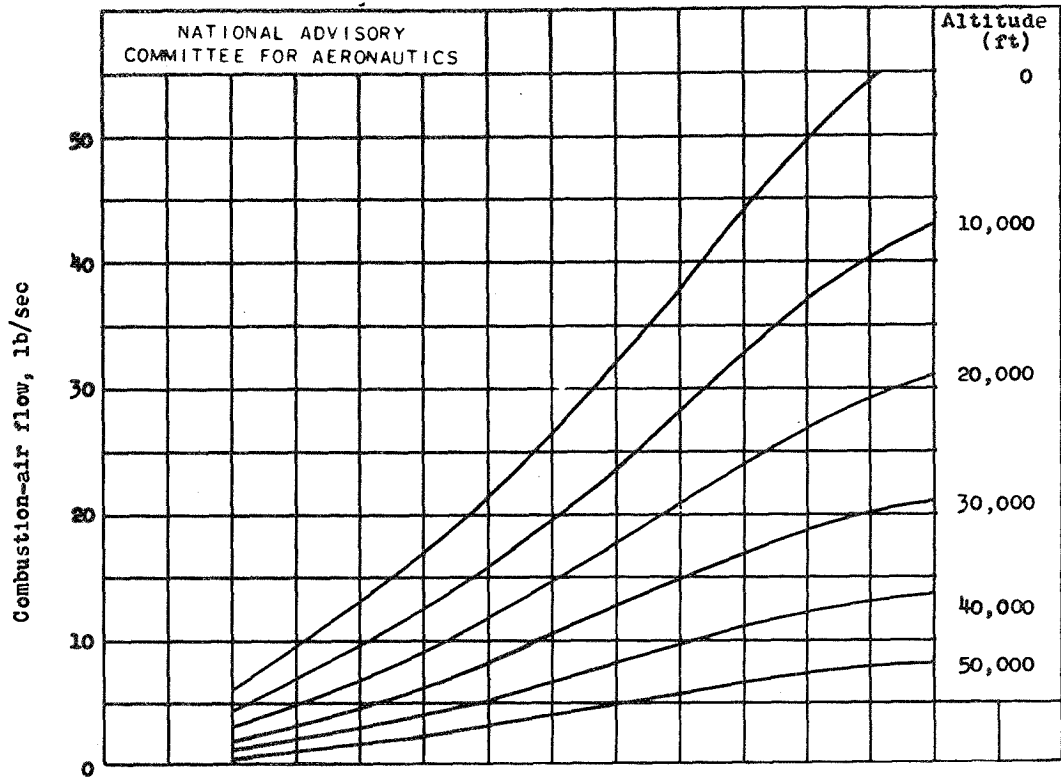


(a) Combustor-inlet total temperature.

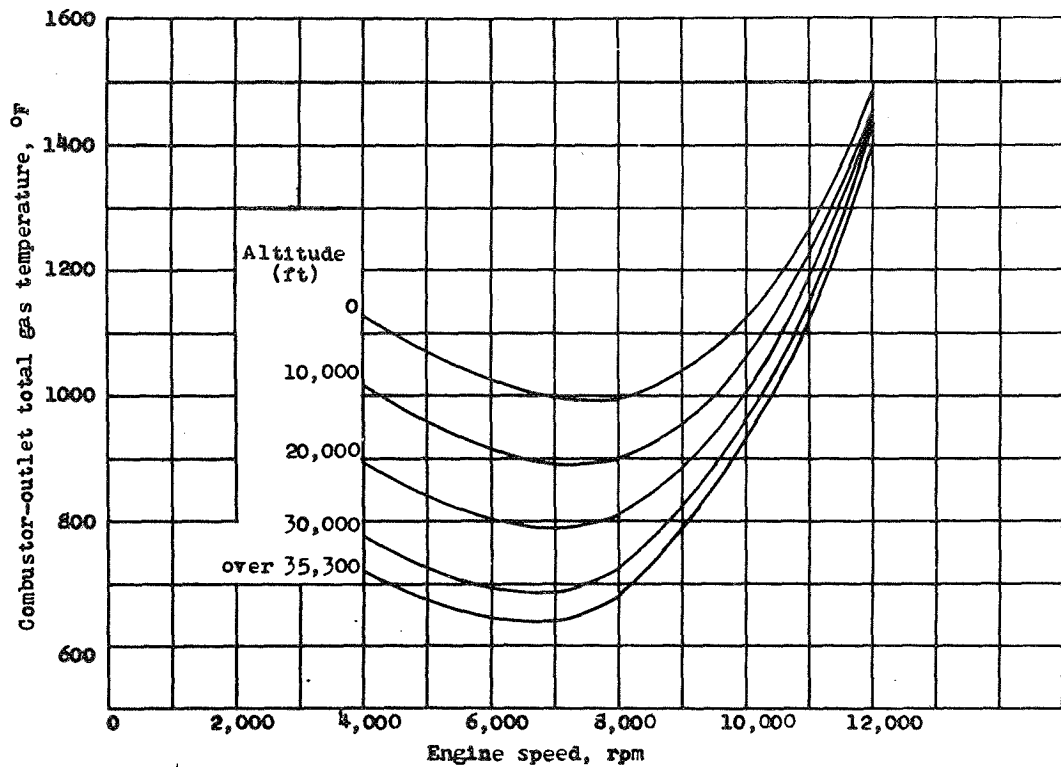


(b) Combustor-inlet total pressure.

Figure 6. - Variation of combustor operating conditions with engine speed for various altitudes at zero ram from performance estimates of the 24C jet engine by the Westinghouse Electric Corporation.



(c) Combustion-air flow.



(d) Required combustor-outlet total gas temperature.

Figure 6. - Concluded. Variation of combustor operating conditions with engine speed for various altitudes at zero ram from performance estimates of the 24C jet engine by the Westinghouse Electric Corporation.

001

NACA RM NO. E6109

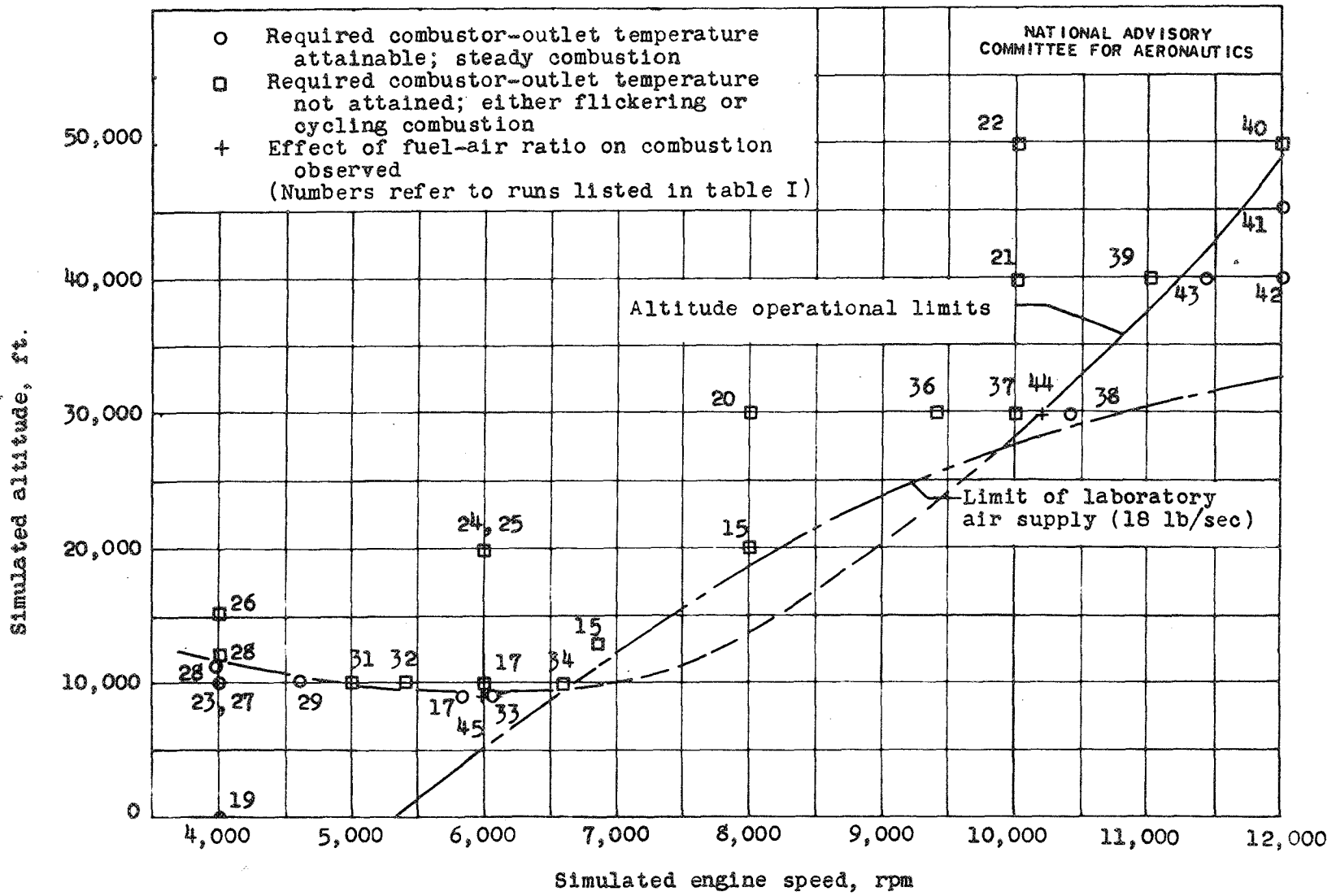
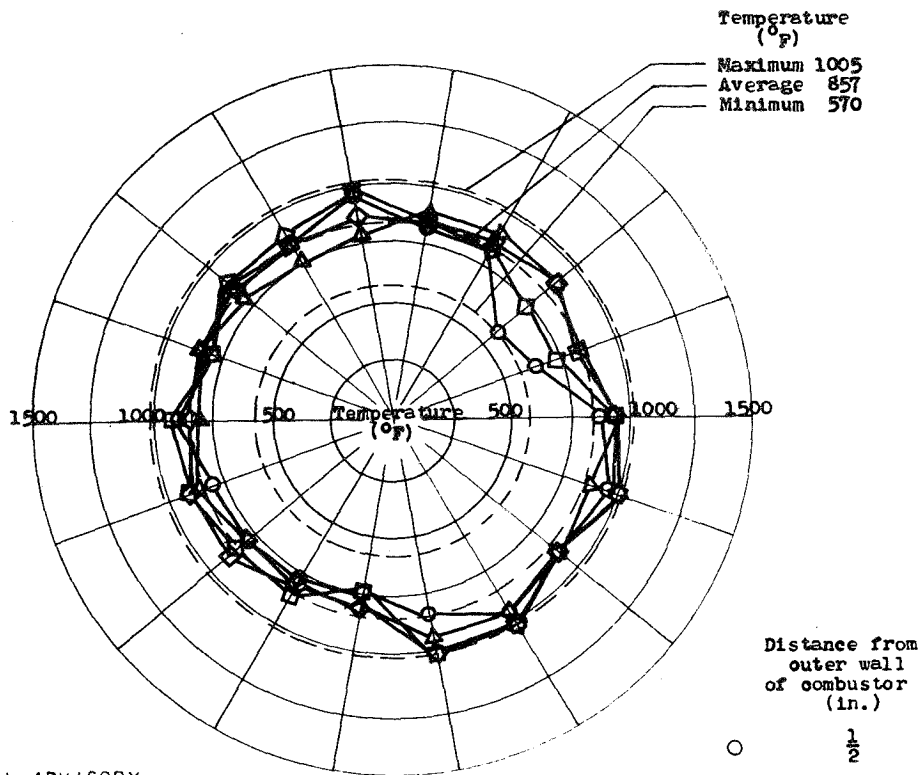


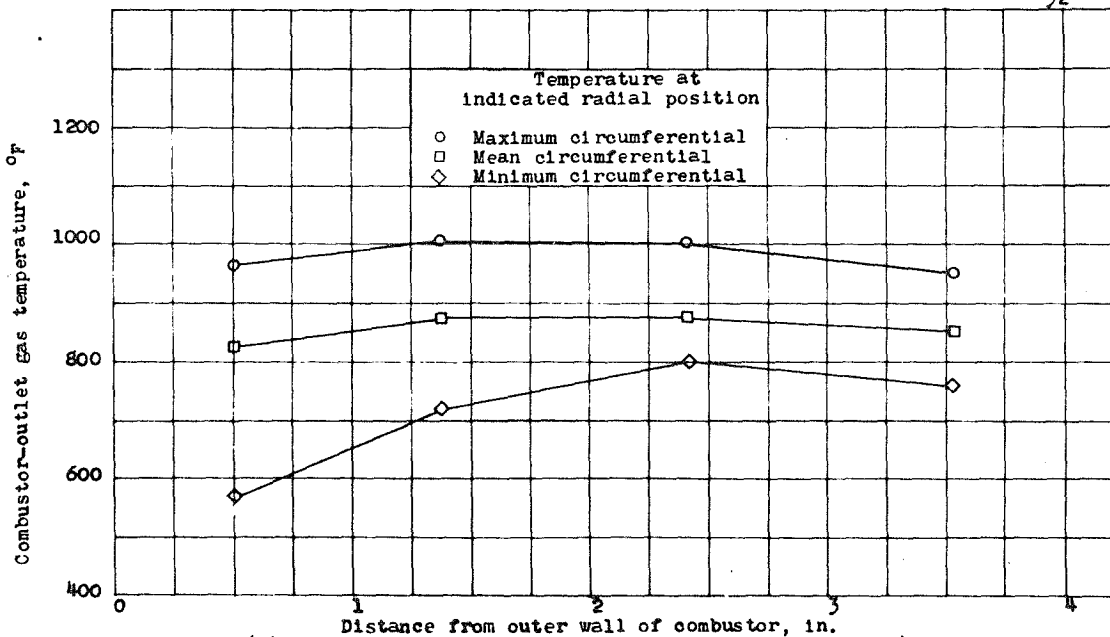
Figure 7. - Altitude operational limits of Westinghouse 24C jet engine for zero ram as determined with 24C-2 combustor.

CONFIDENTIAL



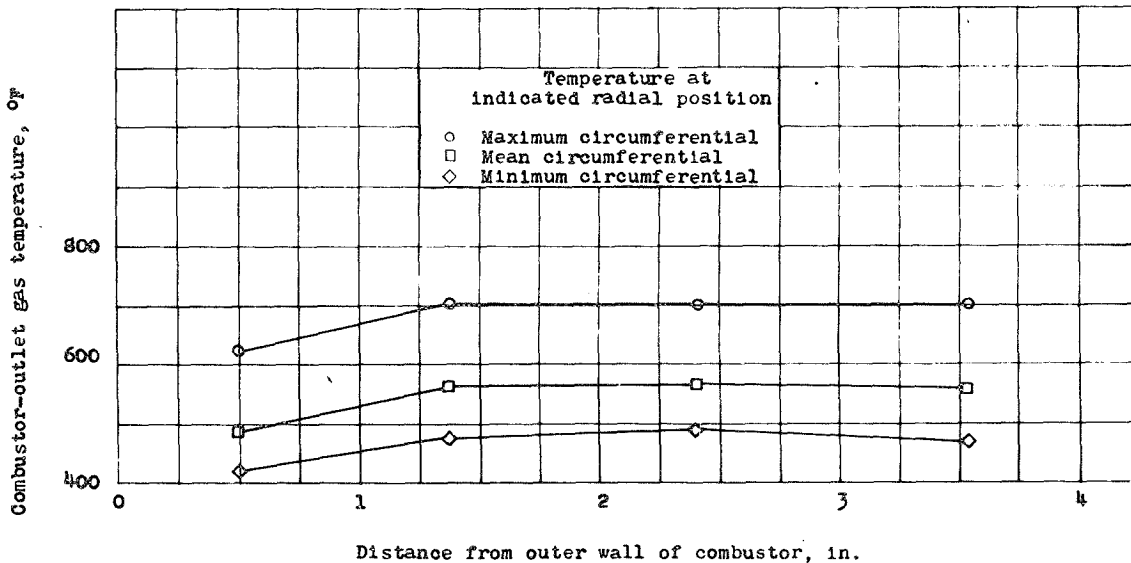
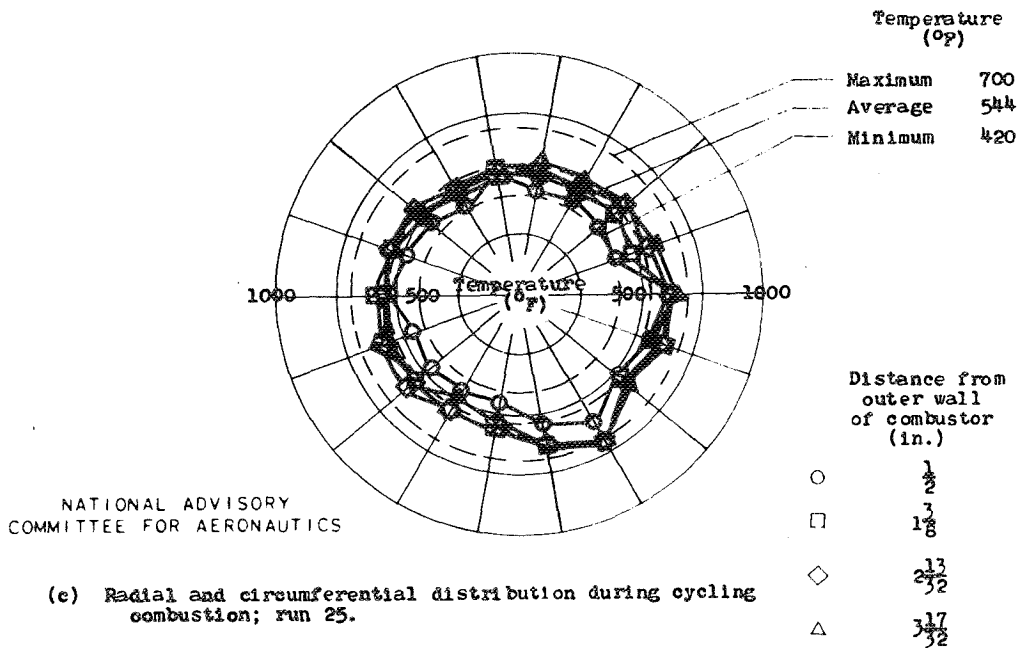
NATIONAL ADVISORY
COMMITTEE FOR AERONAUTICS

(a) Radial and circumferential distribution during steady combustion; run 24.



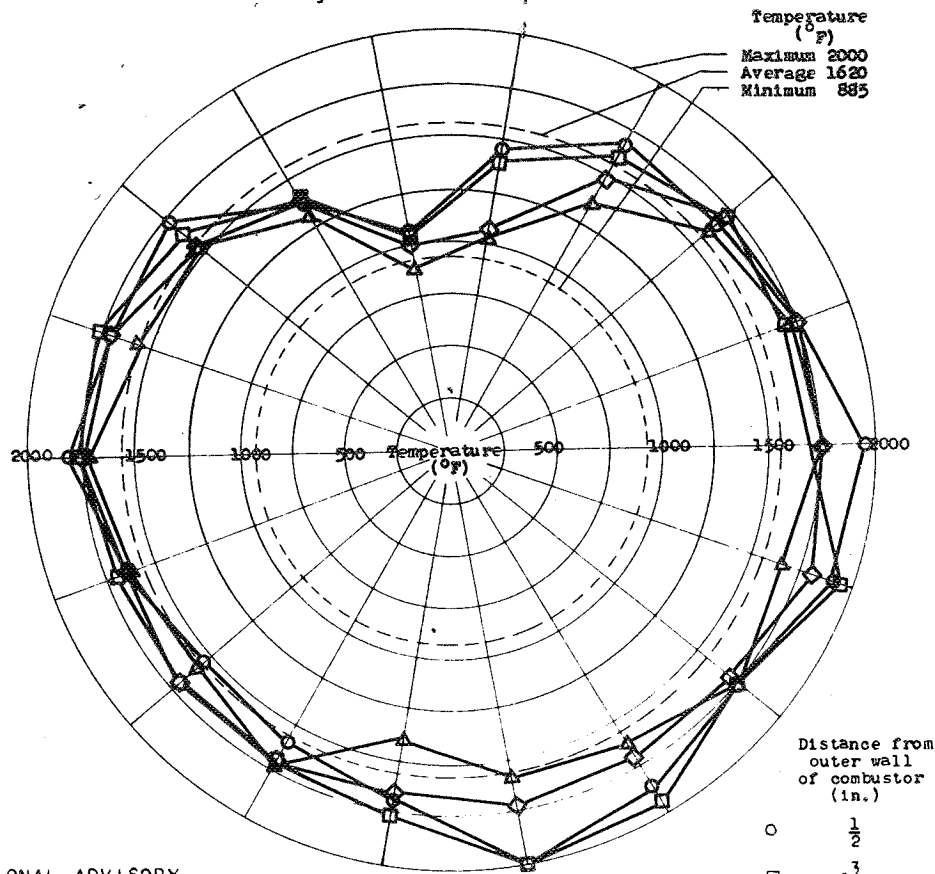
(b) Radial distribution during steady combustion; run 24.

Figure 8. - Temperature distribution at combustor outlet (section C-C, looking upstream) for typical steady and cycling operating conditions from two runs at low inlet-air temperature. Inlet-air temperature, 60° F; Westinghouse 24C-2 combustor.



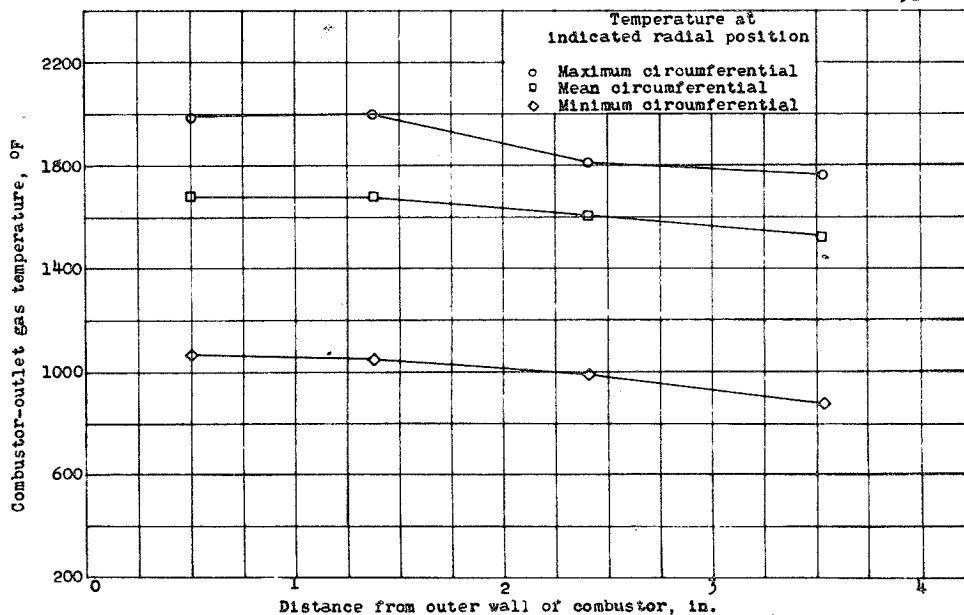
(d) Radial distribution during cycling combustion; run 25.

Figure 8. - Concluded. Temperature distribution at combustor outlet (section C-C, looking upstream) for typical steady and cycling operating conditions from two runs at low inlet-air temperature. Inlet-air temperature, 60° F; Westinghouse 24C-2 combustor.



NATIONAL ADVISORY
COMMITTEE FOR AERONAUTICS

(a) Radial and circumferential distribution during steady combustion; run 42.



(b) Radial distribution during steady combustion; run 42.

Figure 9. - Temperature distribution at combustor outlet (section C-C, looking upstream) for typical steady and cycling operating conditions from two runs at high inlet-air temperature. Inlet-air temperature, 280°F; Westinghouse 24C-2 combustor.

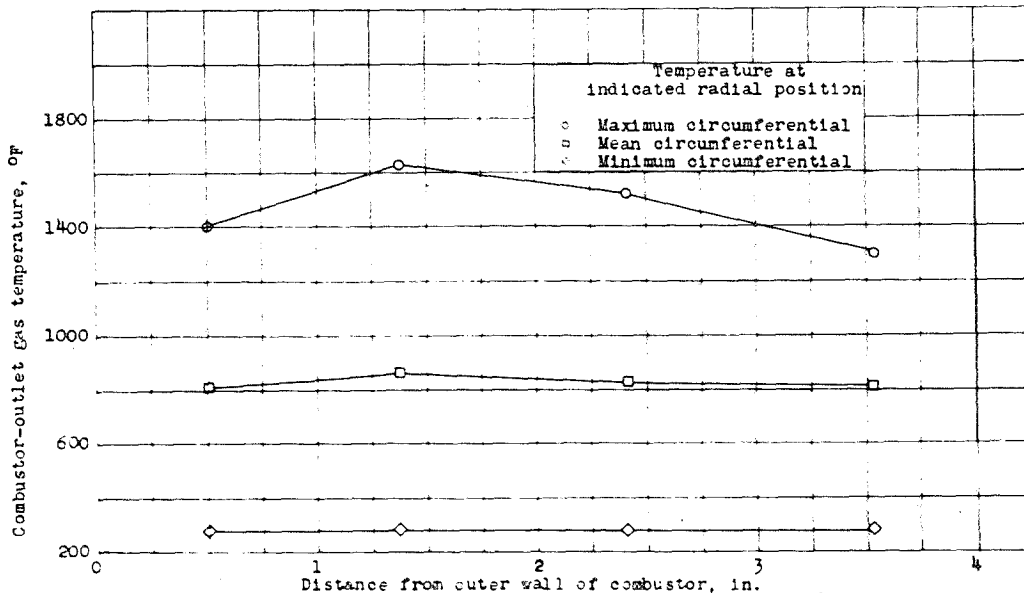
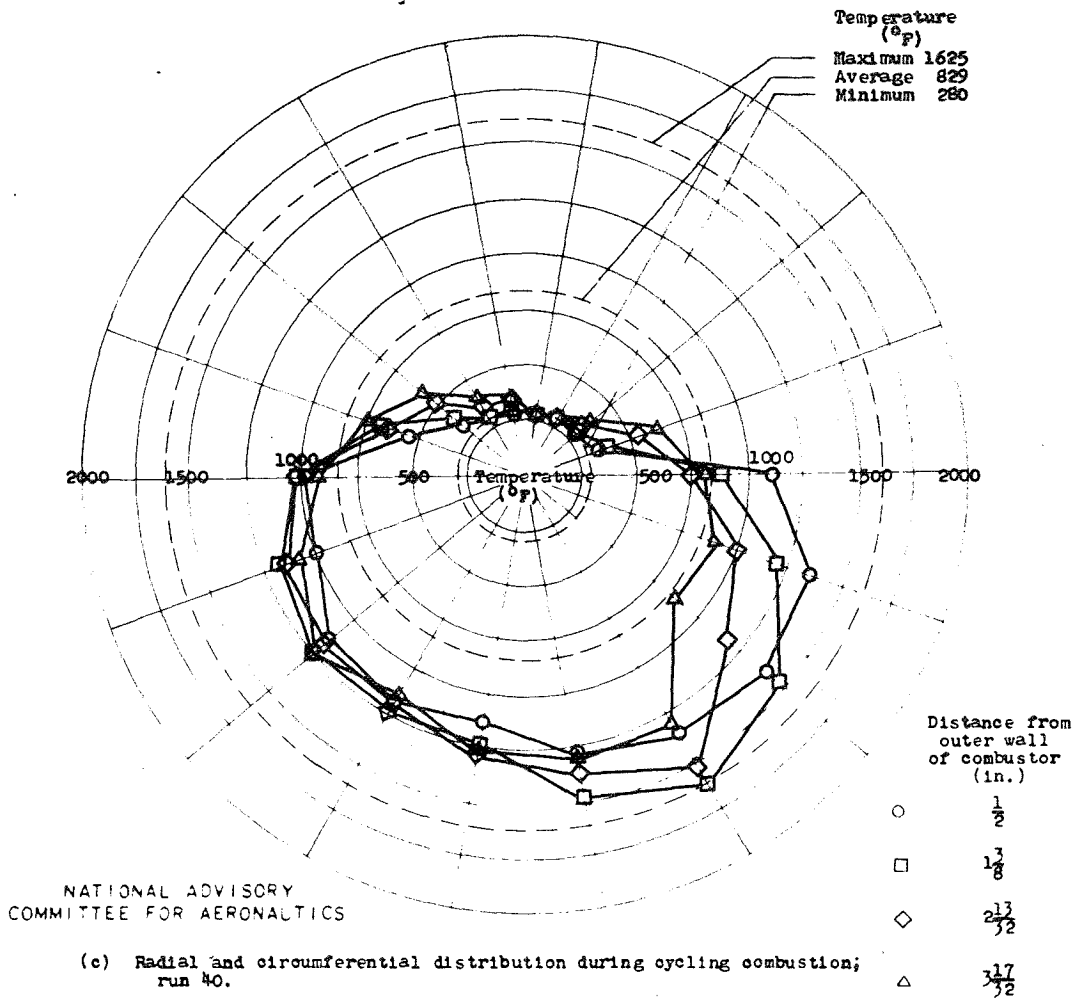


Figure 9. - Concluded. Temperature distribution at combustor outlet (section 3-C looking upstream) for typical steady and cycling operating conditions from two runs at high inlet-air temperature. Inlet-air temperature, 280° F; Westinghouse 24C-2 combustor.

0001

NACA RM No. E6,009

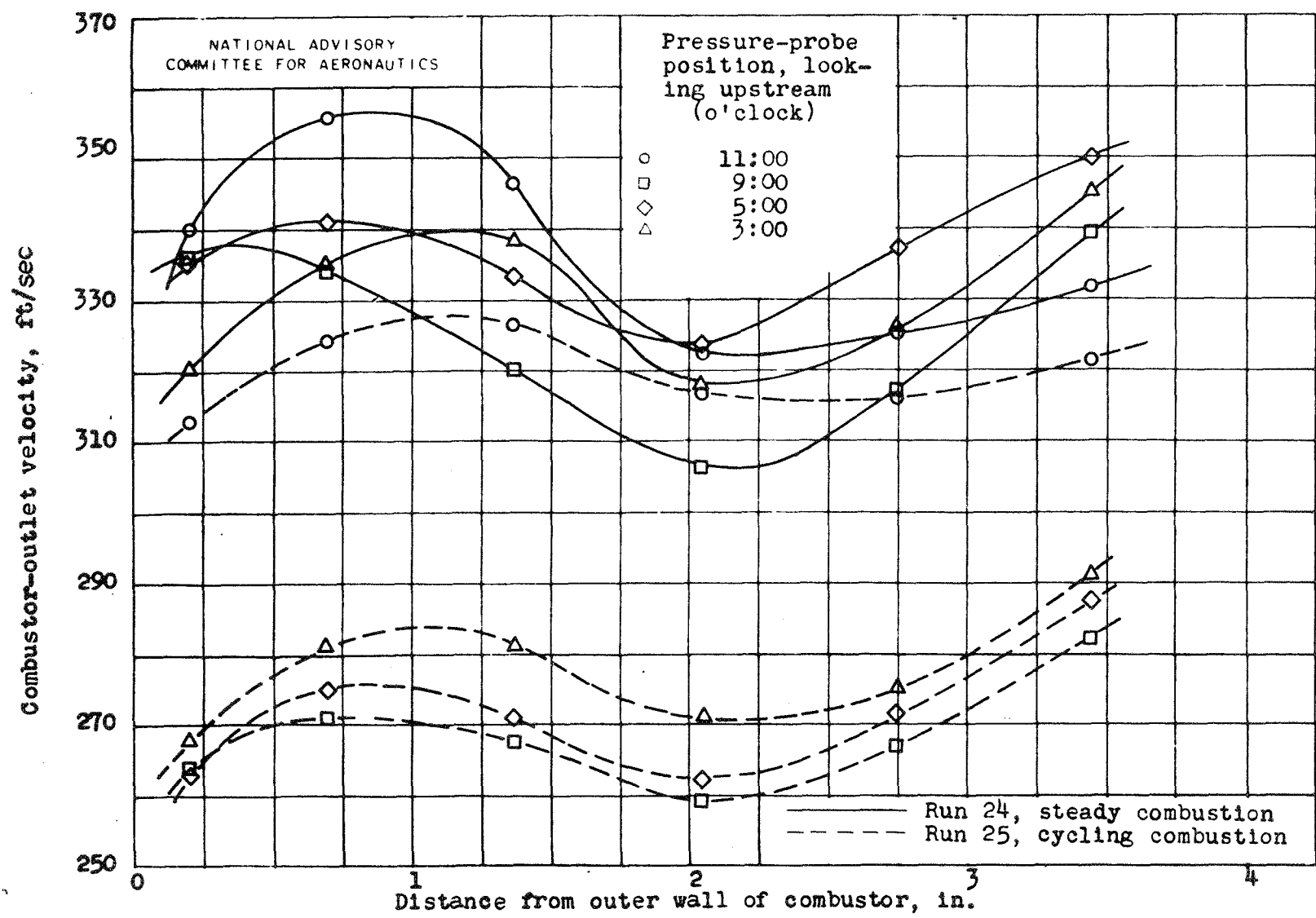
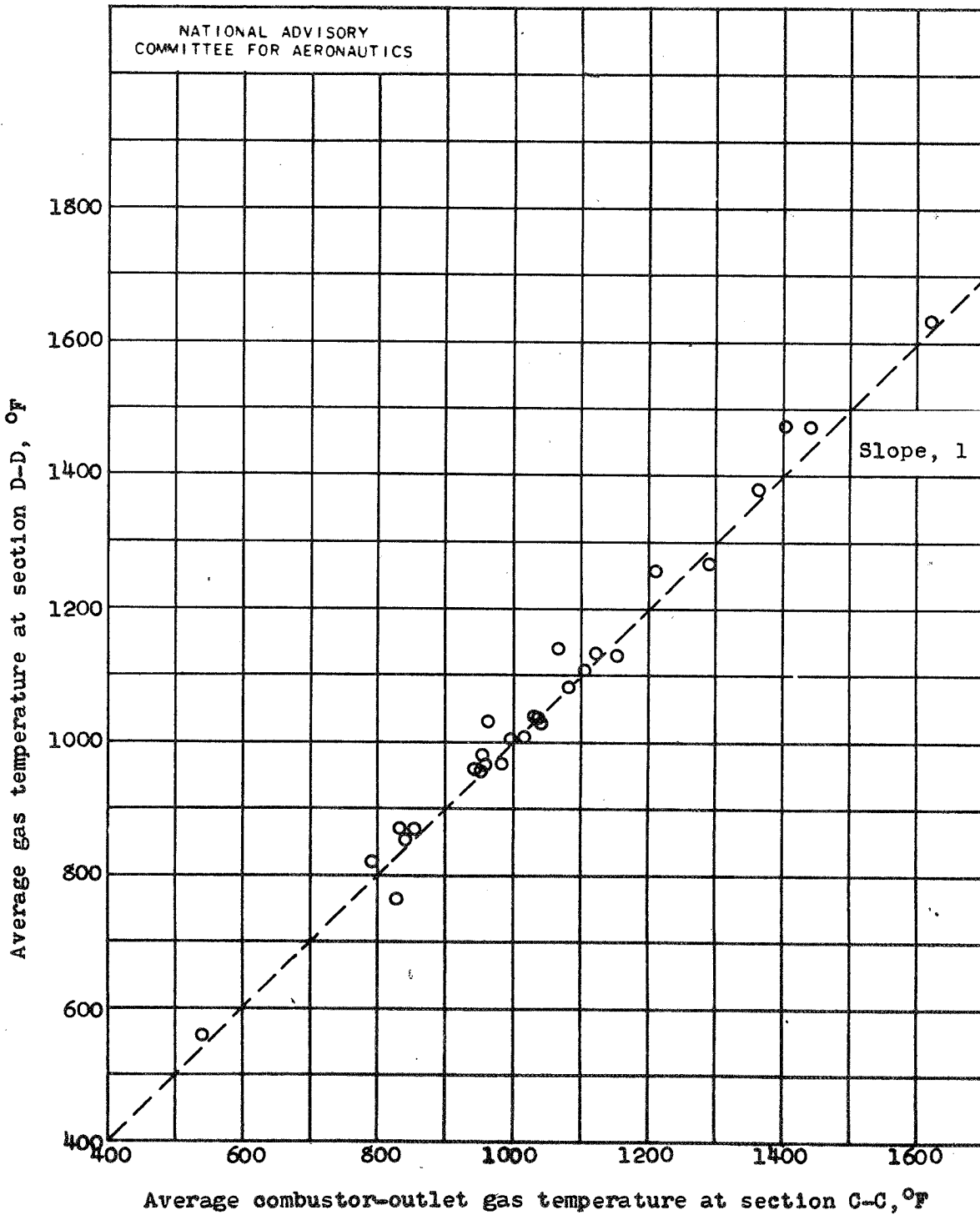


Figure 10. - Velocity distribution at combustor outlet (section C-C) for steady and cycling combustion. Westinghouse 24C-2 combustor.

F-14

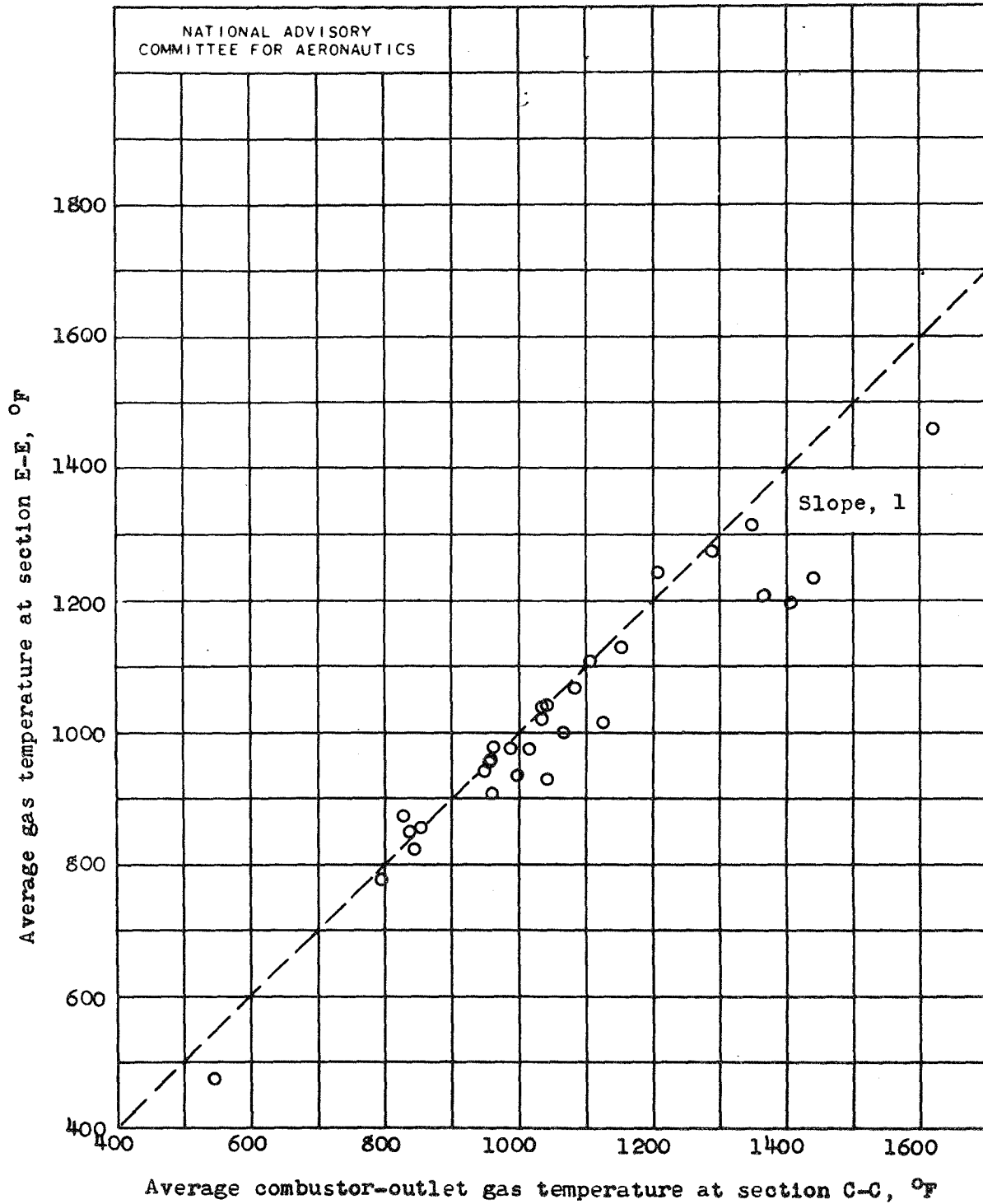
CONFIDENTIAL

CONFIDENTIAL



(a) Section D-D.

Figure 11. - Relation of average gas temperature at sections D-D and E-E to average combustor-outlet gas temperature at section C-C. Westinghouse 24C-2 combustor.



(b) Section E-E.

Figure 11. - Concluded. Relation of average gas temperature at sections D-D and E-E to average combustor-outlet gas temperature at section C-C. Westinghouse 24C-2 combustor.

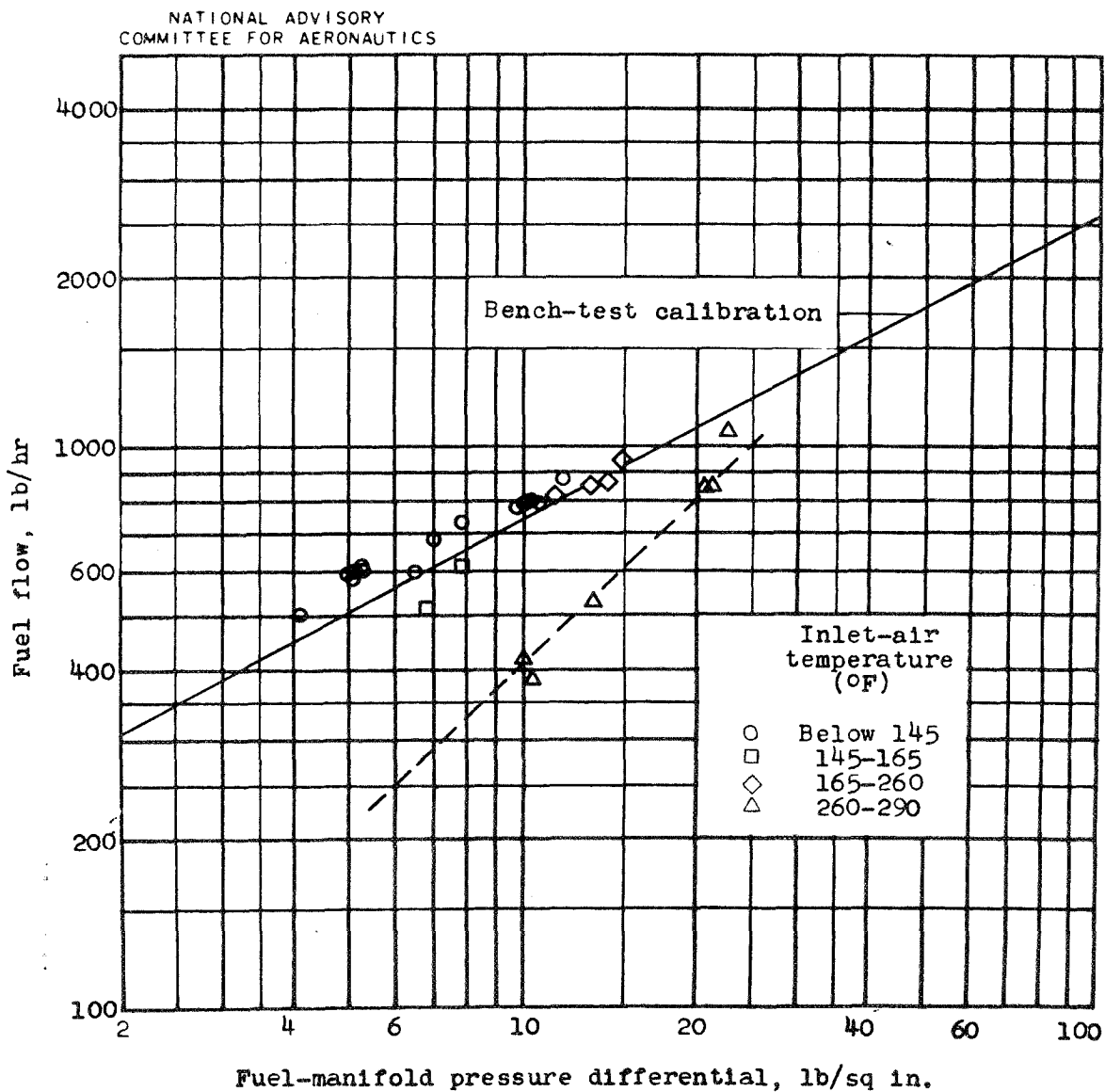


Figure 12. - Variation of fuel flow with fuel-manifold pressure differential. Westinghouse 24C-2 combustor.

044

~~CONFIDENTIAL~~

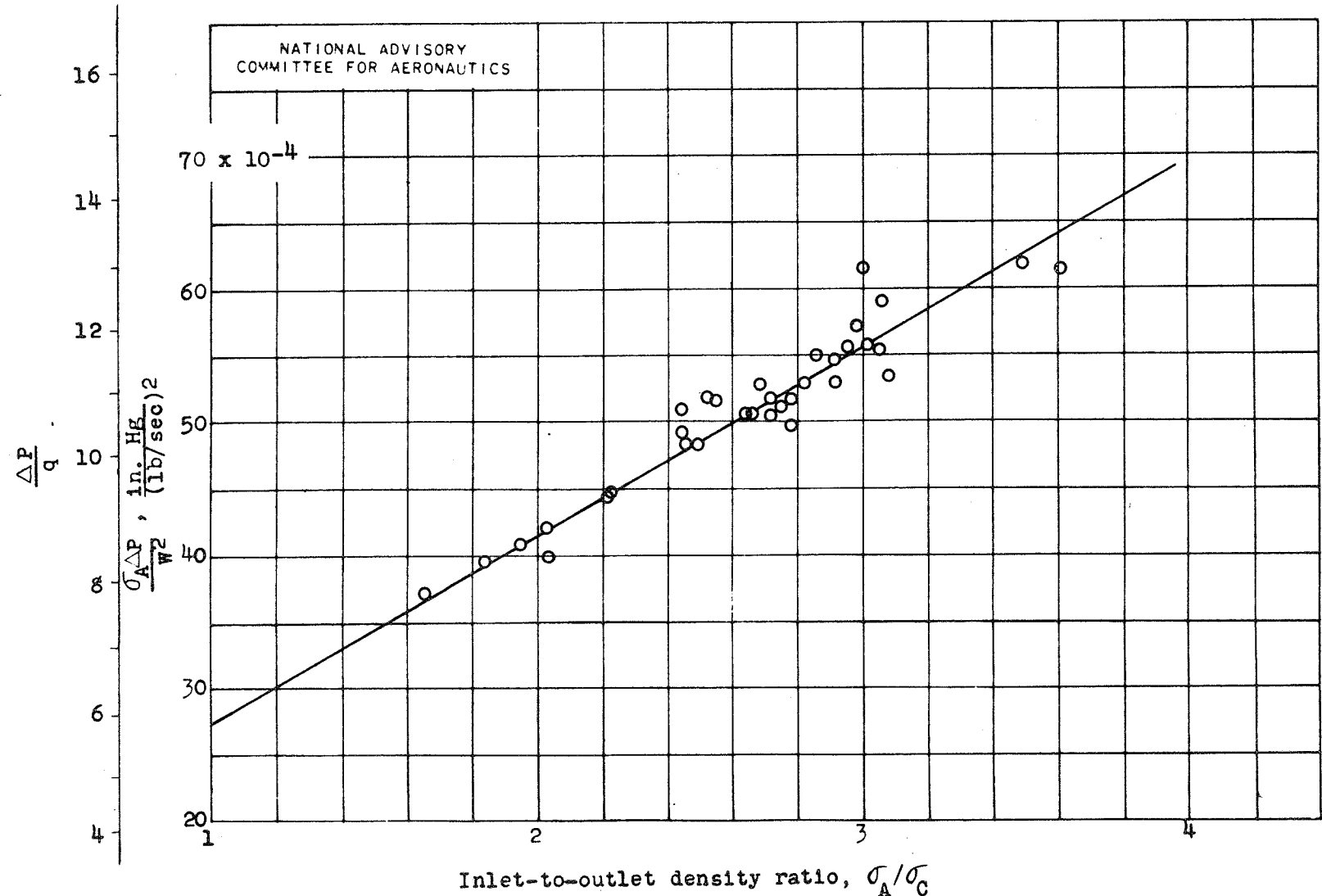


Figure 13. - Correlation of combustor inlet-to-outlet (section A-A to C-C) total-pressure drop. Westinghouse 24C-2 combustor.

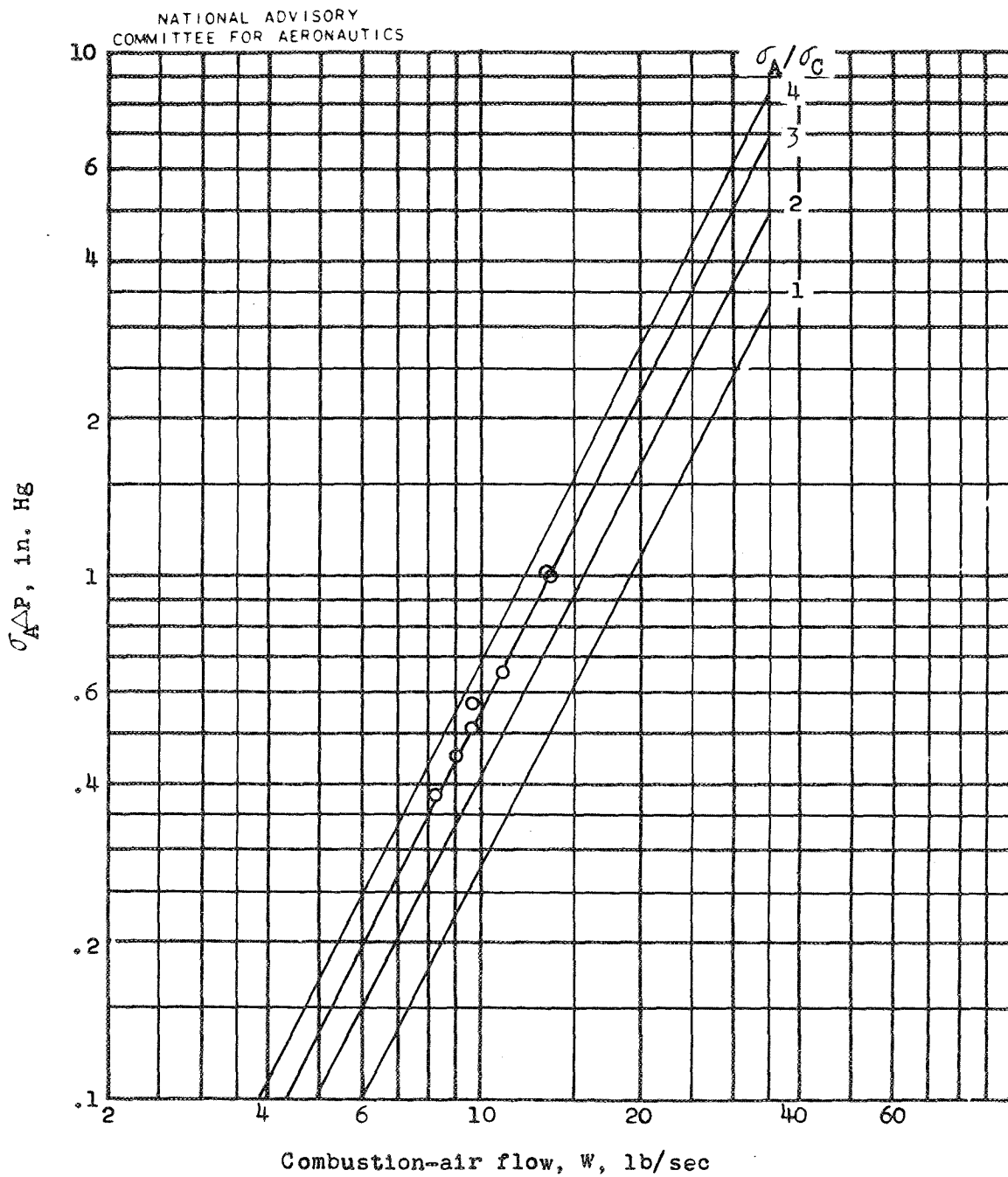
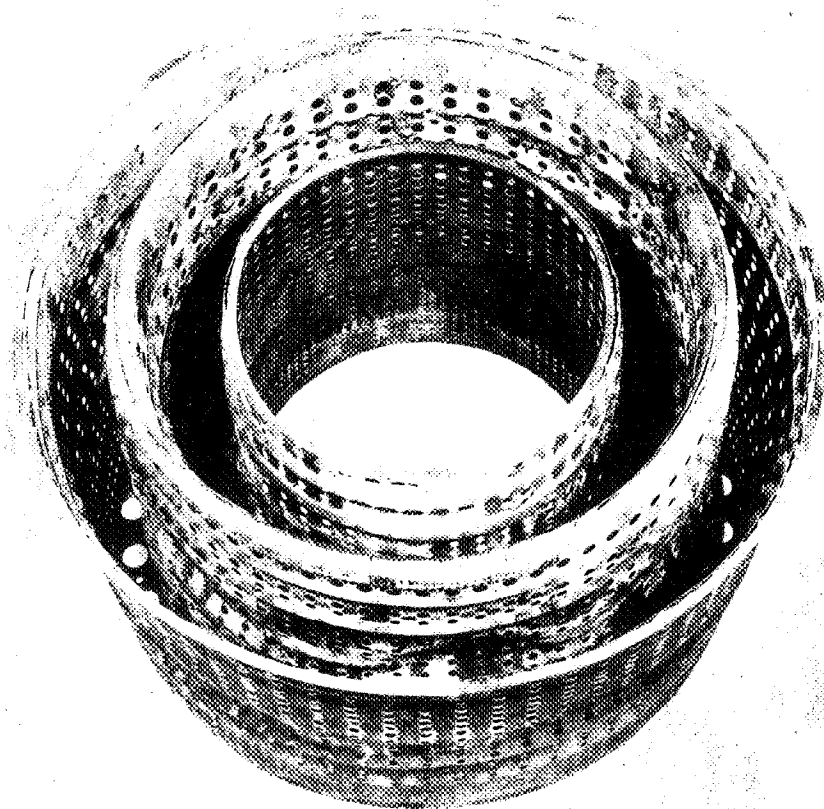
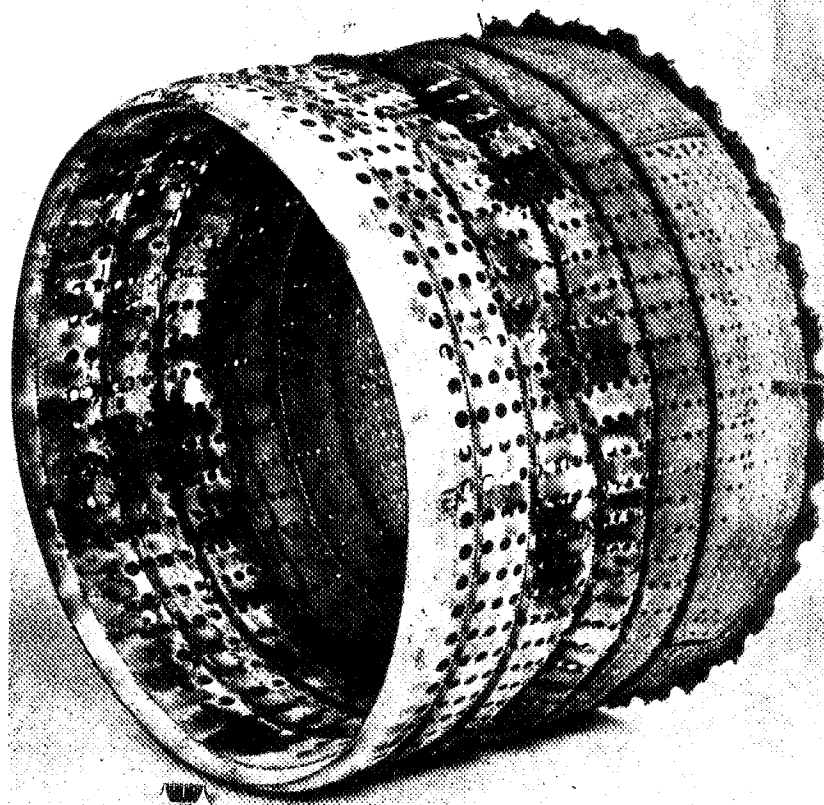


Figure 14. - Combustion-air total-pressure drop from combustor inlet to outlet (section A-A to C-C). Westinghouse 24C-2 combustor.



(a) Entire basket.



(b) Center shell.

NACA
C-15941
9-19-46

Figure 15. - Combustor basket after 29 hours of operation. Westinghouse 24C-2 combustor.